Laterally restrained stainless steel I-section beams under moment gradients: An experimental and numerical study

Song Su[1,2], Zichang Yang[1,2*], Feng Zhou[1,2], Leroy Gardner[3], Guo-Qiang Li[1,2]

[1] *State Key Laboratory of Disaster Reduction in Civil Engineering, Tongji University, Shanghai 200092, China*

[2] *Department of Structural Engineering, Tongji University, 1239 Siping Road, Shanghai 200092, China*

[3] *Department of Civil and Environmental Engineering, Imperial College London, London, UK*

* *Corresponding author. E-mail address: yangzichang@tongji.edu.cn*

Abstract:

Moment gradients have been shown to benefit the local buckling capacities of steel beams, and thus can improve the cross-section design efficiency, which is especially important for stainless steel given its relatively high initial material cost. This paper investigates the local buckling behaviour and design of stainless steel I-section beams under moment gradients. Two four-point bending tests and six three-point bending tests were conducted on the laser-welded ferritic and duplex stainless steel I-section beams, with varying moment gradients taken into consideration. A Digital Image Correlation (DIC) system was employed to monitor the strain development in the upper flanges of the I-section beams during testing. Higher load-carrying capacities were observed in specimens with higher moment gradients. Finite element (FE) models were developed and validated against the test results. Parametric analyses were then conducted, encompassing a range of stainless steel grades, cross-sectional geometries and moment gradients. The ultimate bending moments from the tests and FE simulations were compared with the bending moment resistances predicted by the EC3 provisions and recent design proposals considering moment gradients, which were further developed by incorporation of the Continuous Strength Method (CSM). A reliability analysis was then conducted based on EN 1990. It was shown that the modified CSM, considering the effect of moment gradients, achieved the highest accuracy and adequate reliability among all existing design approaches for stainless steel I-section beams.

Keywords: Beam; Design; Experimental investigation; Local buckling; Moment gradient; Stainless steel; Welded I-section

1 Introduction

Structural steel components are often subjected to point loads and/or uniformly distributed loads, which generate moment gradients along the member length. These moment gradients, in turn, can influence the lateral-torsional and local buckling capacities of the members to varying degrees. The impact of the moment gradients on the lateral-torsional buckling of steel beams has been extensively studied in previous research [1-6]. In ANSI/AISC 360-22 [7], the effects of moment gradients on lateral-torsional buckling capacity are considered by the modification factor C_b. Likewise, in EN 1993-1-1:2022 [8], the effects of moment gradients on the lateral-torsional buckling capacity of steel beams are considered through the moment distribution factor f_M and the normalised slenderness $\bar{\lambda}_{LT}$ when calculating the lateral-torsional buckling reduction factor χ_{LT}.

Early studies into the inelastic local buckling behaviour of steel beams [9-14] showed moment gradients have a significant influence on rotation capacity. Later research experimentally demonstrated the beneficial influence of moment gradients on ultimate load-carrying capacities of steel beams [15-17]. A recent comprehensive investigation into the local buckling capacities of beams under moment gradients was conducted by Yang et al. [18], where digital image correlation (DIC) was utilised to capture the strain development and measure the local buckling half-wavelength of the specimens during testing. A local moment gradient parameter, calculated based on the local buckling half-wavelength, was proposed [19], along with a modified design approach, based on EN 1993-1-1:2022 [8], to allow for the effect of moment gradients. In a subsequent study conducted by Yang et al. [20], the proposed design approach was simplified for practical use by utilising a fixed proportion of the flange width instead of the local buckling half-wavelength to calculate the local moment gradient parameter.

This simplification was shown to provide accurate resistance predictions for I- and hollow section steel beams [20].

Stainless steel is being increasingly widely used in structural engineering due to its excellent ductility, corrosion and fire resistance, low maintenance requirements and aesthetic appeal [21-25]. The fabrication processes for stainless steel structural members typically include cold forming, cold drawing, conventional welding and laser welding. Among these, conventional welding and laser welding are the primary methods utilised for fabricating I-section structural members. Stainless steel exhibits a rounded and continuous stress-strain curve, leading to significant differences in structural response compared to carbon steel. Research therefore is needed to assess the applicability of the design approach proposed by Yang et al. [19,20] to predicting the local buckling resistance of stainless steel I-section beams under moment gradients.

The local buckling behaviour and design of stainless steel I-section beams under moment gradients is investigated in this paper. In Section 2, six three-point bending tests and two four-point bending tests on laser-welded ferritic and duplex stainless steel I-section beams with varying moment gradients are described. In Section 3, the development and validation of finite element (FE) models against the test results is explained; the validated FE models are used for parametric analyses to complement the experimental data, covering several parameters such as different stainless steel grades, cross-sectional geometries and moment gradients. In Section 4, the design approach proposed by Yang et al. [19,20] is introduced and compared with the test results. In Section 5, the applicability of the existing design approaches to stainless steel I-section beams is assessed using 1,227 numerical data points. The existing approach is further extended to be incorporated into the hand calculation expressions of the continuous strength method (CSM) [26], aligning with EN 1993-1-4:2025 [27]. A reliability analysis is finally conducted based on EN 1990:2023 [28].

2 Experimental investigation

2.1 General

Given the limited experimental research on the local buckling behaviour of stainless steel I-section beams under varying moment gradients, a series of experiments, including two four-point bending tests and six stiffened three-point bending tests, were undertaken at the Structural Engineering Laboratory of Tongji University. The I-section beams were fabricated from laser-welded stainless steel plates; two grades of stainless steel – ferritic grade SS430 and duplex grade SS2205 (equivalent to grades EN 1.4016 and EN 1.4462 in EN 1993-1-4:2025 [27], respectively) were considered. The test results are used as benchmark data to validate finite element (FE) models and to assess the design approaches considering moment gradients. Fig. 1 illustrates the notation of the geometric parameters of the test specimens, including the cross-sectional and longitudinal dimensions, where H and B are the height and flange width of the section, respectively, t_f and t_w are the thicknesses of the flange and web, respectively, and L_t, L_s and L_f are the total length, shear span length (for the three-point bending tests) and flexural span length (for the four-point bending tests) of the member, respectively. Additionally, L_{ss} is the shear span length for the four-point bending tests, set to a fixed value of 600 mm, L_{es} is the distance from the edge of the beam to the adjacent stiffener with a value of 100 mm for all the specimens and t_s and t_m are the thickness of the stiffeners arranged at the ends and mid-span of the specimens, which are 10 mm and 18 mm, respectively. The measured geometric properties are summarised in Table 1, in which $\overline{\lambda}_{p,cs}$ is the cross-section slenderness, as defined in Eq. (1), where f_y is the material yield (0.2% proof) strength and $\sigma_{cr,cs}$ is the local buckling stress of the full cross-section determined using CUFSM [29]. The nominal section size of the specimens was 100×100×6×6 (in mm), expressed as "H×B×t_w×t_f". The sections were laser welded in accordance with EN ISO 13919-1:2019 [30], achieving Class B quality, with fillet welds having a nominal leg length of 2.5 mm. The specimens were classified into two series - S4 and

S3, where the label S4 refers to the specimens tested under four-point bending, while the label S3 defines the specimens tested under three-point bending. The two specimens from the S4 series made from SS430 and SS2205 stainless steel, were assigned the numbers 1 and 2, respectively. For the specimens in the S3 series, three shear span lengths – 300 mm, 500 mm, and 700 mm – were adopted for each stainless steel grade. The numbers 1 to 3 were used for the SS430 specimens and the numbers 4 to 6 were used for the SS2205 specimens. In general, the specimens were labelled in the format 'series of specimen – ID of specimen'. For instance, specimen 'S3-1' was made from SS430 stainless steel and subjected to three-point bending with a shear span length of 300 mm.

$$\overline{\lambda}_{\mathrm{p,cs}} = \sqrt{f_{\mathrm{y}}/\sigma_{\mathrm{cr,cs}}} \tag{1}$$

2.2 Material testing

Material coupon tests were carried out to obtain the mechanical properties of the ferritic stainless steel SS430 and duplex stainless steel SS2205 plates prior to structural testing. In Fig. 2, the setup of the coupon tests and the details of the coupons are illustrated. Four coupons, with the dimensions conforming to the requirements of ISO 6892–1 [31], were extracted from each group of stainless steel plate, as shown in Fig. 2b. Monotonic tensile tests were conducted using an MTS machine under displacement control, with strain measurements captured by two strain gauges and an extensometer, as shown in Fig. 2a. The testing strain rate measured by the extensometer conformed to ISO 6892-1 [31] and ASTM E8/E8M-24 [32]. Table 2 provides the material properties for each type of stainless steel, where E is the elastic modulus, f_{y} is the yield strength (0.2% proof stress for stainless steel), f_{u} is the ultimate strength, ε_{u} is the strain at the ultimate strength, ε_{f} is the fracture strain measured over the standard gauge length, and n and m are the strain hardening exponents in the two stage Ramberg–Osgood model [33, 34].

2.3 Geometric imperfection and residual stress measurements

The local buckling resistances of steel structural members are significantly influenced by initial local geometric imperfections, with the most pronounced effect being caused by the longitudinal imperfections [35, 36]. In this study, the longitudinal imperfections were measured in the manner illustrated in Fig. 3. The specimens were placed on a smooth, flat plate and incrementally moved beneath a fixed laser displacement sensor. The imperfections in the specimens were recorded by monitoring the distance changes between the sensor and the specimens along the member length. For each section, measurements over a 300 mm length (greater than twice the local buckling half-wavelength) were taken along three lines in the mid-span region of the top flange, labelled as ω_1 (edge 1), ω_2 (middle line) and ω_3 (edge 2). A typical imperfection distribution for specimen S3-2 is shown in Fig. 3, and the corresponding amplitudes of imperfections (ω_{1m}, ω_{2m} and ω_{3m}) along the three lines (relative to a datum fitted by means of least squares regression) are summarised in Table 3. The maximum measured imperfections were, on average, 55% lower than the permitted essential tolerances specified in EN 1090-2:2018 [37] for welded I-section flanges, where the flange distortion should be less than $B/150$ for sections with a breadth-to-thickness ratio B/t of less than 20.

Residual stresses in laser-welded ferritic and duplex stainless steel I-sections have not been reported before. In this study, the sectioning method was adopted to measure residual stresses in laser-welded ferritic and duplex stainless steel I-sections. Fig. 4 shows the process of the sectioning method and the longitudinal strips after cutting. Two holes, spaced 150 mm apart, were first drilled in line with strip locations. The specimens were then sectioned into a series of longitudinal strips to release the strains. The change in distance between the holes, measured using a demountable mechanical (Demec) strain gauge before and after sectioning, was used to calculate the released strain. Out-of-plane deviations of the longitudinal strips were measured after sectioning, and curvature corrections were applied to the strain values if the deviations exceeded a defined threshold [38, 39]. The residual stress was calculated using

Hooke's Law, and the Young's modulus was obtained from tensile coupon tests. The measured residual stress distributions from the two types of stainless steel I-sections are plotted in Fig. 5. The measured residual stress distributions are generally in good agreement with those proposed in [40] for laser-welded stainless steel I-sections. However, for the flanges and webs of the SS430 section and the webs of SS2205 section, the measured residual stresses were approximately 50% lower than the corresponding proposed distributions, indicating that the predictive model provides conservative estimates for these cases.

2.4 Four-point bending tests

Four-point bending tests were carried out on two stainless steel specimens - S4-1 in ferritic stainless steel and S4-2 in duplex stainless steel. The test setup and the bending moment diagram for the four-point bending tests are shown in Fig. 6a and 6b. The loading configuration of the four-point bending tests was designed to ensure that the beams undergo cross-section failure within the flexural span, i.e., the constant-moment region with zero moment gradient. Vertical load was applied using a 500 kN capacity actuator through a spreader beam, transferring the vertical load to two equal loads acting on the specimens via two steel rollers. Simply-supported boundary conditions were achieved by placing two roller supports symmetrically at the two ends of the beam specimens. Stiffeners were welded and wooden blocks were placed inside the flanges of the beams at the two end supports to prevent localised web failure under the concentrated transverse loads. Lateral supports were provided along the central portion of the specimen at intervals of 150 mm to prevent lateral-torsional buckling. As for the measuring arrangements, linear variable displacement transducers (LVDTs) were used to measure the vertical displacement at the locations of mid-span, the two loading points and the two support points during testing. Additionally, inclinometers, which were placed in the middle of the web at the positions of the two loading rollers and two support points, were employed to measure the in-plane rotations. The values of vertical loads were recorded by load

cells. A speckle pattern was applied to the compression flanges of the specimens in order to provide trackable features, such that the development of strain at the critical regions could be monitored using a DIC system during testing. Due to the obstruction of the field of view caused by the lateral restraints, the DIC system was not configured to capture the deformation of the web in the tests. Nevertheless, all selected sections were expected to be dominated by flange local buckling, as indicated by the calculated elastic plate buckling stresses of the flanges and web. The tests were conducted through displacement-controlled loading. The displacement loading rates were set to ensure that the maximum longitudinal compressive strain rate remained below 0.05% min^{-1}. The tests were terminated when either the loads decreased to 90% of their maximum value or the specimens exhibited excessive deformation.

Typical failure modes are shown in Fig. 7. For the four-point bending specimens, the local buckling failure was observed within the flexural length, as shown in Fig. 7a for specimen S4-1. The normalised bending moment M/M_{pl} is plotted against the normalised average curvature along the flexural length κ/κ_{pl} for specimens S4-1 and S4-2 in Fig. 8a, where M is the bending moments within the flexural length, calculated following the procedure set out in [41], M_{pl} is the plastic bending moment resistance calculated from Eq. (2), W_{pl} is the plastic section modulus, κ is the average curvature along the flexural length determined from Eq. (3), θ_{f1} and θ_{f2} are the measured rotations at the two loading points, κ_{pl} is the elastic curvature of the specimens at M_{pl} calculated from Eq. (4) and I is the second moment of area.

$$M_{pl} = f_y W_{pl} \tag{2}$$

$$\kappa = \frac{|\theta_{f,1}| + |\theta_{f,2}|}{L_f} \tag{3}$$

$$\kappa_{pl} = \frac{M_{pl}}{EI} \tag{4}$$

It can be seen from Fig. 8a that the duplex stainless steel beam exhibited lower rotation capacity compared to the ferritic stainless steel beam, primarily attributed to the higher cross-

section slenderness. The development of longitudinal strain obtained from DIC in the compression flange is shown for a typical specimen, specimen S4-1, in Fig. 9a. The key results from the four-point bending tests are summarised in Table 4, where M_u is the ultimate bending moment capacity and κ_u is the corresponding ultimate average curvature.

2.5 Stiffened three-point bending tests

Three-point bending tests were carried out on six stainless steel specimens reinforced by stiffeners at the mid-span loading point, namely S3-1, S3-2, and S3-3 for the ferritic stainless steel cross-sections, and S3-4, S3-5, and S3-6 for the duplex stainless steel cross-sections. The specimens were designed to have the same nominal cross-section geometries while being subjected to different moment gradients. The test setup and bending moment diagram for the stiffened three-point bending tests are shown in Fig. 6c and 6d. Vertical loads were applied through an extended stiffener at mid-span - see Fig. 6c - this arrangement stiffened the beam against localised web failure and allowed sufficient space for the DIC measurements of the top flange. Simply-supported boundary conditions were achieved by placing two roller supports symmetrically at the two ends of the beams. Web stiffeners were welded to the beams at the support points to prevent localised web failure. Lateral bracing and instrumentation were configured in the same manner as those in the four-point bending tests, and the same loading procedure was followed.

All three-point bending specimens failed by inelastic local buckling adjacent to the mid-span stiffener, as shown in Fig. 7b for the typical case of specimen S3-4. The normalised bending moment M/M_{pl} is plotted against the normalised average end rotation θ/θ_{pl} for specimens S3-1 to S3-6 in Fig. 8b, where θ represents average end rotation of θ_{f1} and θ_{f2}, and θ_{pl} represents the elastic end rotation when the specimen reached the plastic bending moment resistance M_{pl}, as defined by Eq. (5).

$$\theta_{pl} = \frac{M_{pl}L_s}{4EI} \tag{5}$$

The duplex stainless steel beams exhibited lower normalised rotational capacities than the ferritic stainless steel beams due to their higher cross-section slenderness, but similar normalised load-carrying capacities compared to the ferritic stainless steel beams with the same shear span length. The latter observation is explained by the higher strain hardening exhibited by duplex stainless steel [42]. With reducing shear span, the moment capacities of the specimens generally increased, indicating the beneficial effect of moment gradients on the local buckling capacity of stainless steel beams. A typical illustration of the development of compressive strain in the top flange of the beams, shown for specimen S3-4, as monitored by DIC, including at the stages of the initiation and spread of plasticity, and at the ultimate load, is presented in Fig. 9b. The key results from the stiffened three-point bending tests are summarised in Table 4, where M_u is the ultimate bending moment resistance and θ_u is the corresponding ultimate end rotation.

3 Finite element modelling and parametric analysis

3.1 General

In this section, the establishment of finite element (FE) models of laser-welded stainless steel I-section beams under moment gradients using the FE software ABAQUS [43] is presented, as detailed in Section 3.2 and 3.3. The developed models are then validated against test results in Section 3.4. Extensive parametric studies on welded stainless steel I-section beams are then presented, considering different cross-section slenderness values, aspect ratios, shear span lengths and loading configurations, as described in Section 3.5.

3.2 Basic modelling assumptions

The 4-node shell element with reduced integration (S4R) [43] was employed to model the I-section beams. A mesh size of $b_f/16 \times b_f/16$ (referring to 'length × width' of the shell element) was adopted, where b_f is the minimum width of the flat plates. Based on the method proposed in [44], the thicknesses of two elements at each end of the web were increased to model the

fillet radii. An initial mesh sensitivity study was conducted using element sizes of $b_f/4$, $b_f/8$, $b_f/12$, $b_f/16$ and $b_f/32$, as shown in Table 5. The results indicate that an element size of $b_f/16$ provides consistent and accurate results with reasonable computational efficiency. General multi-point constraints (∗MPC) were used to create the connection between the end nodes in the web and corresponding nodes in the flange, avoiding the overlapping of elements. It is noted that the mesh modelling strategies have been confirmed to be accurate and effective in the simulation of the local buckling behaviour of thin-walled steel and stainless steel members reported in previous studies [45-50].

As illustrated in Fig. 10, the cross-sections at the loading and support points of the member were coupled to reference points, with suitable boundary conditions applied. The cross-sections at both ends were constrained with pinned in-plane and fixed out-of-plane boundary conditions, achieved by restraining the translational degrees of freedom in the Y- and Z-directions and the rotational degrees of freedom about the X- and Y-axes at the reference points. Vertical loads were applied to the reference points of the cross-sections at the loading locations, with the translational degree of freedom in the Z-direction and the rotational degrees of freedom about the X- and Y-axes restrained. An additional restraint in the X-direction was applied at one of the loading points. The I-sections were laterally restrained to replicate the experimental setup accurately. The NLGEOM command [43] was utilised in the FE simulations to incorporate the effects of geometrical nonlinearity.

3.3 Material properties, geometric imperfections and residual stresses

The engineering stress-strain curves of the ferritic stainless steel SS430 and duplex stainless steel SS2205 obtained from the tensile coupon tests were converted into true stress-strain curves and subsequently adopted in the developed FE models to simulate the material behaviour. Initial local geometric imperfections were introduced into the FE models using the lowest eigenmode to represent the local imperfection shape [51], as obtained from a linear

bifurcation analysis. The local imperfection amplitudes were taken as those measured in the tests, while global imperfections were not applied since lateral-torsional buckling was restrained during the tests. The residual stress distributions proposed in [40] for laser-welded stainless steel I-sections were adopted in the developed FE models. A comparison of the FE analysis results obtained using the measured residual stresses and the predicted residual stress distributions proposed in [40] is presented in Fig. 11. It can be observed that the difference between the measured and predicted residual stress distributions has a negligible effect on the load-carrying capacity of the sections.

3.4 Validation of FE model

The test-to-FE ratios of ultimate bending moment capacities $M_{u,test}/M_{u,FE}$ for all specimens are presented in Table 6. The mean values of $M_{u,test}/M_{u,FE}$ for the specimens under four-point bending and stiffened three-point bending are 1.036 and 1.015, respectively, and the corresponding CoV values are 0.002 and 0.017, respectively. In Fig. 12, a typical M/M_{pl}-κ/κ_{pl} curve for a beam (specimen S4-1) under four-point bending and M/M_{pl}-θ/θ_{pl} curve for a beam (specimen S3-1) under stiffened three-point bending obtained from the FE analyses are compared with those from the corresponding tests; the failure modes from the FE models and tests are also presented. It can be seen from Fig. 12 that the bending moment responses and failure modes of the FE results agree well with the benchmark test results described in Section 2.4 and 2.5. It can be concluded that the local buckling behaviour of ferritic and duplex stainless steel I-section beams under moment gradients can be accurately captured by the developed FE models, demonstrating the accuracy and consistency of the FE modelling strategies.

3.5 Parametric studies

Parametric studies were conducted to understand further the performance of welded stainless steel I-section beams under moment gradients and to generate data over a wider

parameter range. The key parameters considered in the parametric studies were stainless steel grade, cross-section slenderness, cross-section aspect ratio, shear span length and loading configuration. The investigated material grades were austenitic stainless steel grade EN 1.4301, ferritic stainless steel grade EN 1.4016 and lean duplex stainless steel grade EN 1.4462. The two-stage Ramberg-Osgood model was utilised to describe the stress-strain response, with the basic material parameters obtained from [52] and detailed in Table 7. The cross-section slenderness was determined using numerical tools (i.e., CUFSM [29]) and varied from 0.2 to 1.1. Cross-section aspect ratios of 1, 1.5 and 2 were considered. Shear span lengths ranging from 100 mm to 5000 mm were studied, representing different levels of moment gradients. Three loading configurations were considered: beams under pure bending (equivalent to the central portion of the four-point bending setup), as well as stiffened and unstiffened three-point bending. The models, which utilised symmetric boundary conditions to enhance computational efficiency, are shown in Fig. 13. The local imperfection amplitudes in the beams were set equal to $b_c/250$, where b_c is the flat width of the critical plate [27]. This value has been shown to be accurate, with a suitable degree of conservatism through the comparative analyses reported in [19]. The residual stress distribution model proposed by Yuan et al. [53] for welded stainless steel I-sections was adopted. A total of 1,227 models were analysed, with 409 models for each of the pure bending, stiffened three-point bending and unstiffened three-point bending configurations.

4. Existing design approach considering the effect of moment gradients

4.1 General

The cross-sectional design of steel I-section beams, considering the effect of moment gradients, has been investigated by Yang et al. [19,20]. In this section, the developed design approach is summarised and its applicability to the stainless steel I-section beams is assessed based on the test results. In Section 4.2, the local moment gradient parameter is introduced. An

overview of the provisions in EC3 and the modified design procedure are then provided in Section 4.3. Finally, the provisions in EC3 and the modified design procedure considering moment gradient effects are evaluated against the test results in Section 4.4.

4.2 Local moment gradient parameter

A local moment gradient factor C_l was defined to describe the effect of moment gradients in the proposed design approach [19], as given by:

$$C_1 = \begin{cases} \dfrac{2\left|M_{\mathrm{Ed}} - M_{1,\mathrm{Ed}}\right|}{M_{\mathrm{pl}}}, & \text{for stiffened cross-sections} \\ \dfrac{\left|M_{\mathrm{Ed}} - M_{1,\mathrm{Ed}}\right|}{M_{\mathrm{pl}}}, & \text{for unstiffened cross-sections} \end{cases} \tag{6}$$

where M_{Ed} refers to the bending moment at the considered point and $M_{1,\mathrm{Ed}}$ represents the bending moments at a specific distance either side of the considered point. The specific distance was initially proposed to be determined by using the local buckling half-wavelength L_b calculated using either analytical formulae [54] or numerical tools like CUFSM [29]. For stiffened cross-sections, the specific distance is equal to L_b. For unstiffened cross-sections, the specific distance is equal to half of L_b. The determination of the local moment gradient factor C_l was further simplified by Yang et al. [20] through the utilisation of fixed portions of the flange width B (i.e., 1.25B for carbon steel I-sections) instead of the local buckling half-wavelength L_b as the specific distance, as shown in Fig. 14. It should be noted that the local moment gradient parameter C_l and the ultimate moment capacity should be calculated based on the moment values on both sides of the considered point, with the more conservative result being adopted as the design resistance. More details of the local moment gradient factor C_l can be found in [19], where several different load cases are included.

4.3 Modifications to the EC3 framework

The cross-section design approach for stainless steel beams subjected to combined bending and shear specified in EN 1993-1-4:2025 [27] follows that set out for steel beams in

EN 1993-1-1:2022 [8]. For stainless steel beams not susceptible to shear buckling (i.e., the height-to-thickness ratio of the web h_w/t_w does not exceed the limit of $52\varepsilon/\eta$ [27, 55], where ε is the material parameter and η is the constant value of 1.20) under combined shear and bending, the design bending moment M_{Ed} should satisfy Eq. (7), where $M_{c,Rd}$ is the design bending moment resistance of the cross-section and $M_{v,Rd}$ is the design bending moment resistance of the cross-section reduced by the presence of high shear force.

$$M_{\mathrm{Ed}} \le \min\left(M_{\mathrm{c,Rd}}, M_{\mathrm{V,Rd}}\right) \tag{7}$$

The design bending moment resistance $M_{c,Rd}$ is calculated using Eq. (8), where W is the section modulus defined by Eq. (9) based on the classification of the cross-section and γ_{M0} is the partial factor for cross-section design, with a value of 1.10 for stainless steel. The terms W_{pl}, W_{el} and W_{eff} are the plastic section modulus, elastic section modulus and effective section modulus, respectively.

$$M_{\mathrm{c,Rd}} = \frac{W f_{\mathrm{y}}}{\gamma_{\mathrm{M0}}} \tag{8}$$

$$W = \begin{cases} W_{\mathrm{pl}} & \text{for Class 1 and 2} \\ W_{\mathrm{el}} & \text{for Class 3} \\ W_{\mathrm{eff}} & \text{for Class 4} \end{cases} \tag{9}$$

The plastic moment resistance reduced by the presence of high shear force $M_{V,Rd}$ is calculated using Eq. (10), where η_V is taken as 0.5 based on EN 1993-1-4:2025 [27], $f_{y,red}$ is the reduced yield strength, which is calculated using Eqs. (11) and (12) and $W_{pl,V}$ and $W_{pl,nV}$ are the plastic modulus of the regions of the cross-section influenced and not influenced by shear (essentially the web and flanges), respectively.

$$M_{\mathrm{V,Rd}} = \begin{cases} W_{\mathrm{pl}} f_y / \gamma_{M0}, & \text{for } V_{\mathrm{Ed}} \le \eta_V V_{\mathrm{pl,Rd}} \\ \left(W_{\mathrm{pl,V}} f_{y,\mathrm{red}} + W_{\mathrm{pl,nV}} f_y\right) / \gamma_{M0}, & \text{for } \eta_V V_{\mathrm{pl,Rd}} < V_{\mathrm{Ed}} \le V_{\mathrm{pl,Rd}} \end{cases} \tag{10}$$

$$f_{y,\mathrm{red}} = (1-\rho) f_y \tag{11}$$

$$\rho = \left(\frac{2V_{\mathrm{Ed}}}{V_{\mathrm{pl,Rd}}} - 1 \right)^2 \tag{12}$$

The design procedures for stainless steel beams under combined bending and shear, as set out in EN 1993-1-4:2025 [27] and in the modified design approach proposed by Yang et al. [19], are shown in Fig. 15. The modified design approach simplifies the calculation process by combining $M_{\mathrm{c,Rd}}$ and $M_{\mathrm{v,Rd}}$ into a modified design resistance under combined moment and shear $M_{\mathrm{mod,V,Rk}}$, as given by Eq. (13) and Eq. (14). A strength enhancement factor κ_{Cl}, calculated using Eq. (15), which is a function of the local moment gradient parameter C_{l}, is introduced to quantify the effect of moment gradients. Note that, the susceptibility of the cross-section to web crippling should also be duly assessed in accordance with EN 1993-1-4:2025 [27].

$$M_{\mathrm{Ed}} \le M_{\mathrm{mod,V,Rd}} \tag{13}$$

$$M_{\mathrm{mod,V,Rd}} = \begin{cases} \kappa_{\mathrm{Cl}} W f_{\mathrm{y}} / \gamma_{\mathrm{M0}} & \text{for } V_{\mathrm{Ed}} \le \eta_{\mathrm{V}} V_{\mathrm{pl,Rd}} \\ \kappa_{\mathrm{Cl}} \left(W_{\mathrm{V}} f_{\mathrm{y,red}} + W_{\mathrm{nV}} f_{\mathrm{y}} \right) / \gamma_{\mathrm{M0}} & \text{for } \eta_{\mathrm{V}} V_{\mathrm{pl,Rd}} < V_{\mathrm{Ed}} \le V_{\mathrm{pl,Rd}} \end{cases} \tag{14}$$

$$\kappa_{C1} = 1 + 0.15 C_1 \tag{15}$$

4.4 Evaluation against test results of stainless steel I-section beams

The aforementioned design methods have been shown to be effective for carbon steel I-section beams under moment gradients, but validation is still required for stainless steel I-section beams. The normalised ultimate bending moment resistances of the specimens in S3 series $M_{\mathrm{u}}/M_{\mathrm{u,uniform}}$ are plotted against the local moment gradient parameter C_{l} in Fig. 16, where $M_{\mathrm{u,uniform}}$ represents the tested ultimate bending moment resistances of the corresponding specimens in the S4 series under zero moment gradient. It can be observed that the $M_{\mathrm{u}}/M_{\mathrm{u,uniform}}$

values increase as the local moment gradient parameter C_l increases, indicating the beneficial influence of moment gradients on the local buckling resistance of stainless steel beams.

The normalised ultimate moment $M_u/M_{c,Rd}$ is plotted against the normalised ultimate shear force $V_u/V_{pl,Rd}$ for test specimens S3-1 to S3-6, together with the interaction curves of normalised bending moment-shear force based on the provisions in EC3 and the proposed design procedure [19], as shown in Fig. 17. It can be observed that the proposed design method yields more accurate predictions of on the cross-section resistances of stainless steel I-section beams under moment gradients, compared to the EC3 provisions.

5. Extension of the Continuous Strength Method (CSM)

5.1 General

In this section, the developed to capture the influence of moment gradients is incorporated into the hand calculation expressions of the Continuous Strength Method (CSM). The applicability of the design approach to stainless steel I-section beams is assessed using 1,227 data points from the parametric studies. Finally, a reliability analysis is presented in Section 5.4 based on EN 1990 D:2023 [28].

5.2 Incorporation of developed approach into CSM expressions

The traditional design approach set out in EN 1993-1-4:2025 [27], as well as the proposals Yang et al. [19,20], despite the latter capturing the effect of moment gradients, remain overly conservative when applied to the design of stainless steel I-section beams because of the neglect of strain hardening. Strain hardening is systemically accounted for in the CSM [26, 56-58] is included in a number of international design standards, including ASCE 8-22 [59], AISC 370-21 [60,61] and EN 1993-1-4:2025 [27]. The effect of moment gradients is also captured when the CSM is used in the framework of design by geometrically and materially nonlinear analysis with imperfections (GMNIA) [62, 63], but not in the CSM resistance functions for

413 hand calculations. An approach that incorporates the moment gradient effect into the CSM
414 resistance expressions is therefore proposed and evaluated in this section.

415 For stainless steel, the CSM cross-section strain limits for hand calculations are
416 determined from Eq. (16), where ε_{csm} is the CSM strain limit, $\varepsilon_y = f_y/E$ is the elastic strain at
417 the yield stress, ε_u is the ultimate strain, $\bar{\lambda}_{p,cs}$ is the cross-section slenderness, Ω is the upper
418 bound multiple of the yield strain (with a recommended value of 15) and C_1 is a material
419 coefficient [64].

420
$$\frac{\varepsilon_{csm}}{\varepsilon_y} = \begin{cases} \frac{0.25}{\bar{\lambda}_{p,cs}^{3.6}} \le \min\left(\Omega, \frac{C_1\varepsilon_u}{\varepsilon_y}\right) & \text{for} \quad \bar{\lambda}_{p,cs} \le 0.68 \\ \left(1 - \frac{0.222}{\bar{\lambda}_{p,cs}^{1.050}}\right)\frac{1}{\bar{\lambda}_{p,cs}^{1.050}} & \text{for} \quad 0.68 < \bar{\lambda}_{p,cs} \le 1.0 \end{cases} \tag{16}$$

421 Under the combined actions of bending moment and shear force, a reduced CSM strain
422 limit $\varepsilon_{csm,V}$ is applied, as given by Eq. (17) [65], where ρ is the vertical shear force reduction
423 factor calculated using Eq. (12) and $\mu_{y,fl}$ is the ratio of elastic bending resistance of the cross-
424 section considering the flanges alone M_{fl} to the elastic bending resistance of the full cross-
425 section $M_{el,y}$, as given by Eq. (18).

426
$$\varepsilon_{csm,V} = \varepsilon_{csm} - \rho(\varepsilon_{csm} - \mu_{y,fl}\varepsilon_y) \tag{17}$$

427
$$\mu_{y,fl} = \frac{M_{fl}}{M_{el,y}} \tag{18}$$

428 The bending resistance, allowing for the effect of shear, is determined from Eq. (19) [26],
429 where $M_{csm,V,Rd}$ is the cross-section bending resistance considering shear, γ_{M0} is the partial
430 safety factor for cross-section resistance, E_{sh} is the strain hardening modulus and α is the CSM
431 bending parameter, with a value of 2.0 for I-sections in bending about the major axis.

$$M_{csm,V,Rd}=\begin{cases}\dfrac{W_{el}f_y}{\gamma_{M0}}\dfrac{\varepsilon_{csm,V}}{\varepsilon_y} & \text{for} \quad \dfrac{\varepsilon_{csm,V}}{\varepsilon_y} < 1.0 \\ \dfrac{W_{pl}f_y}{\gamma_{M0}}\left[1+\dfrac{E_{sh}}{E}\dfrac{W_{el}}{W_{pl}}\left(\dfrac{\varepsilon_{csm,V}}{\varepsilon_y}-1\right)-\dfrac{1-\frac{W_{el}}{W_{pl}}}{\left(\frac{\varepsilon_{csm,V}}{\varepsilon_y}\right)^{\alpha}}\right] & \text{for} \quad \dfrac{\varepsilon_{csm,V}}{\varepsilon_y} \geq 1.0\end{cases} \tag{19}$$

The aforementioned equations can be extended consider the effect of moment gradients, as given by Eq. (20), in which κ_{Cl} is the strength enhancement parameter, calculated using Eq. (15).

$$M_{csm,V,mod,Rd}=\begin{cases}\kappa_{Cl}\dfrac{W_{el}f_y}{\gamma_{M0}}\dfrac{\varepsilon_{csm,V}}{\varepsilon_y} & \text{for} \quad \dfrac{\varepsilon_{csm,V}}{\varepsilon_y} < 1.0 \\ \kappa_{Cl}\dfrac{W_{pl}f_y}{\gamma_{M0}}\left[1+\dfrac{E_{sh}}{E}\dfrac{W_{el}}{W_{pl}}\left(\dfrac{\varepsilon_{csm,V}}{\varepsilon_y}-1\right)-\dfrac{1-\frac{W_{el}}{W_{pl}}}{\left(\frac{\varepsilon_{csm,V}}{\varepsilon_y}\right)^{\alpha}}\right] & \text{for} \quad \dfrac{\varepsilon_{csm,V}}{\varepsilon_y} \geq 1.0\end{cases} \tag{20}$$

5.3 Evaluation of design approaches

The accuracy of the different design approaches for stainless steel I-section beams is assessed using 1227 data points from the FE parametric studies in this section. The results are shown in Fig. 18, in which the normalised ultimate moment M_u / $M_{c,Rd}$ is plotted against the normalised ultimate shear force V_u / $V_{pl,Rd}$ based on the results obtained from the FE models, along with the design provisions from EC3, the modified design procedure with the moment gradient calculated using L_b and 1.25*B*, and the proposed modified CSM. It can be observed that the CSM resistance expressions, incorporating the strength enhancement parameter for moment gradients, effectively capture the observed behaviour. The results obtained from the modified design procedure using L_b and 1.25*B* are comparable and demonstrate greater accuracy than the traditional EC3 design provisions, indicating the applicability of the design approaches to stainless steel I-section beams. Fig. 18 also shows that the maximum beneficial effect of moment gradients, after accounting for the reduction caused by shear stresses, is observed when $V_{Ed}/V_{pl,Rd}$ is close to 0.75. The adverse effect of shear stresses begin to outweigh the beneficial effect of moment gradients at higher levels of shear.

Fig. 19 illustrates the definition of the normalised shear-moment angle θ, where θ is defined in Eq. (21). The FE-to-predicted ultimate bending moment resistance ratios $M_{\mathrm{u,FE}}$ / $M_{\mathrm{u,pred}}$ are plotted against the normalised shear-moment angle θ in Fig. 20.

$$\theta = \tan^{-1}\left(\frac{V_u / V_{\mathrm{pl,Rd}}}{M_u / M_{\mathrm{pl,Rd}}}\right) \tag{21}$$

The mean and CoV values for M_{u} / $M_{\mathrm{u,pred}}$ are presented in Table 8. The mean values for M_{u} / $M_{\mathrm{u,pred}}$ for the stiffened three-point bending cases obtained from the EC3 provisions, the modified design procedure using L_{b} and using 1.25B and the modified CSM are 1.401, 1.321, 1.323 and 1.197, respectively, and the corresponding CoV values are 0.095, 0.082, 0.082 and 0.088, respectively. For the unstiffened three-point bending cases, the mean values for M_{u} / $M_{\mathrm{u,pred}}$ obtained from the EC3 provisions, the modified design procedure using L_{b} and using 1.25B and the modified CSM are 1.274, 1.260, 1.261 and 1.140, respectively, and the CoV values are 0.072, 0.070, 0.070 and 0.076, respectively. The modified CSM expressions are shown to provide more accurate resistance predictions than the traditional EN 1993-1-4:2025 approach and the modified design procedure using L_{b} and using 1.25B, while consistently remaining on the safe side.

5.4 Reliability analysis

The reliability of the modified CSM expressions, the modified EN 1993-1-4:2025 approach with the specified distance of 1.25B and the traditional EN 1993-1-4:2025 approach for stainless steel I-section beams under stiffened and unstiffened three-point bending is assessed in this section based on the Annex D of EN 1990:2023 [28]. A target reliability index β = 3.8 and a target cross-section partial safety factor γ_{M0} = 1.1 [27] were adopted for stainless steel design considering a 50-year design life. Tables 9 and 10 list the key statistical parameters of the material and geometric properties, in accordance with [66], where $f_{\mathrm{y,mean}}/f_{\mathrm{y,nom}}$, $f_{\mathrm{u,mean}}/f_{\mathrm{u,nom}}$ and $X_{\mathrm{mean}}/X_{\mathrm{nom}}$ represent the mean-to-nominal ratios of yield strength, ultimate

strength and geometric properties, respectively, and V_{fy} and V_X denote the coefficients of variation of the yield strength and geometric properties, respectively. The mean value correction factor b of the benchmark results (numerical simulation data) to the design approaches was calculated using Eq. (22) from [67].

$$b = \frac{1}{n}\sum_{i=1}^{n}\frac{r_{e,i}}{r_{t,i}} \tag{22}$$

Based on the recommendations of Afshan et al. [66], the yield strength f_y and section modulus W_{Rk} were selected as the basic variables. These variables were used in the function defined by Eq. (23) to represent the key factors influencing the cross-section resistance of beams. The dependency of the resistance on the basic variables (captured through the exponents c and d) for each design approach was determined as detailed in [66]. The coefficient of variation (CoV) of the basic variables V_{rt} was determined using Eq. (24), where V_{WRk} represents the CoV of the section modulus, derived from statistical factors of the related geometric parameters [65]. Note that the fabrication quality of laser-welded may justify the use of lower geometric variability though the necessary data to confirm this are not currently available. The required partial safety factors γ^*_{M0}, along with the CoV of the error term V_δ and the CoV of the overall resistance function V_r, were calculated in accordance with Annex D of EN 1990:2023 [28].

$$M_{c,Rd} = k\, f_y^{\,c} W_{Rk}^{\,d} \tag{23}$$

$$V_{rt} = \sqrt{(cV_{fy})^2 + (dV_{WRk})^2} \tag{24}$$

The required partial safety factor γ^*_{M0}, as well as the ratios of the required partial safety factors to the target value of γ_{M0}=1.1(i.e. $\gamma^*_{M0}/\gamma_{M0}$), along with the statistical analysis factors b, V_δ and V_r for each design approach are presented in Table 11. From Table 11, it can be

observed that all design approaches have a partial safety factor ratio less than unity and therefore satisfy the Eurocode reliability requirement, as was the case when the revised material overstrength factors set out in [68] were adopted. The modified CSM expressions exhibit the mean value correction factor *b* closest to unity, highlighting their superior accuracy. This approach is therefore recommended for implementation in future structural design standards and practice.

6 Conclusions

The local buckling behaviour and cross-section design of stainless steel I-section beams under moment gradients have been investigated experimentally and numerically. In total, two four-point bending tests and six stiffened three-point bending tests were conducted on laser-welded ferritic and duplex stainless steel I-section beams, considering different moment gradients. The development of strain in the upper flanges of the I-sections in the mid-span regions of the beams was measured using a DIC system during testing. The test results showed that stainless steel I-section beams under higher moment gradients tend to have higher load-carrying capacities.

Finite element models of stainless steel I-section beams under moment gradients were then developed and validated against the test results. Parametric analyses were subsequently conducted, covering a variety of stainless steel grades, cross-sectional geometries and moment gradients. A total of 1,227 FE results were generated. The FE results also showed increasing bending capacity with increasing moment gradient, caused by the restraint provided by the less heavily loaded regions of the beams to the point of maximum moment, until high shear forces became dominant, at which point capacities reduced. Stocky cross-sections, which are widely employed in engineering practice, typically exhibited the greatest capacity benefits under moment gradients.

The ultimate bending moments from the test results and FE simulations were compared with the bending moment resistances calculated according to the existing provisions in EC3 for stainless steel I-section beams and recent design proposals considering the effect of moment gradients. The existing proposed approach was further extended to be incorporated into the CSM, aligning with EN 1993-1-4:2025 [27]. A reliability analysis was conducted based on EN 1990 D:2023 [28]. The modified CSM expressions, which considered the effect of moment gradients, showed the highest accuracy and satisfied the Eurocode reliability requirements. For application in practice, the developed proposals can be readily coded in design software and simplified tables for C_l can be established.

Acknowledgements

Financial support from the National Natural Science Foundation of China (Project No. 52020105004) and the Shanghai Municipal Administration of Talent Affairs (Project No. 24PJD123) is gratefully acknowledged.

References

[1] D'Aniello M, Landolfo R, Piluso V, Rizzano G. Ultimate behavior of steel beams under non-uniform bending. Journal of Constructional Steel Research 2012;78:144–58. https://doi.org/10.1016/j.jcsr.2012.07.003.

[2] White DW, Duk Kim Y. Unified flexural resistance equations for stability design of steel I-section members: Moment gradient tests. Journal of Structural Engineering 2008;134:1471–86. https://doi.org/10.1061/(ASCE)0733-9445(2008)134:9(1471).

[3] Sawyer HA. Post-Elastic Behavior of Wide-Flange Steel Beams. Journal of the Structural Division 1961;87:43–71. https://doi.org/10.1061/JSDEAG.0000733.

[4] Lay MG, Galambos TV. Inelastic Beams under Moment Gradient. Journal of the Structural Division 1967;93:381–99. https://doi.org/10.1061/JSDEAG.0001589.

[5] Lukey AF, Adams PF. Rotation Capacity of Beams under Moment Gradient. Journal of the Structural Division 1969;95:1173–88. https://doi.org/10.1061/JSDEAG.0002290.

[6] Kucukler M, Gardner L, Macorini L. Lateral–torsional buckling assessment of steel beams through a stiffness reduction method. Journal of Constructional Steel Research 2015;109:87–100. https://doi.org/10.1016/j.jcsr.2015.02.008.

[7] American Institute of Steel Construction (AISC). AISC 360-22: Specification for Structural Steel Buildings. Chicago, IL: AISC; 2022.

[8] European Committee for Standardization (CEN). EN 1993-1-1:2022, Eurocode 3 – Design of steel structures – Part 1-1: General rules and rules for buildings. Brussels: CEN; 2022.

[9] Lay MG. The Experimental Bases for Plastic Design: A Survey of the Literature. Fritz Engineering Laboratory Report No. 297.3, Department of Civil Engineering, Lehigh University, Bethlehem, PA, USA.

[10] Lay MG, Galambos TV. The Inelastic Behavior of Beams under Moment Gradient. Fritz Engineering Laboratory Report No. 297.12, Department of Civil Engineering, Lehigh University, Bethlehem, PA, USA.

[11] Lay MG. Some Studies of Flange Local Buckling in Wide-Flange Shapes. Journal of the Structural Division, ASCE, 91(ST6), and Fritz Engineering Laboratory Report No. 195, Department of Civil Engineering, Lehigh University, Bethlehem, PA, USA.

[12] Lay MG, Galambos TV. Inelastic Beams under Moment Gradient. Journal of the Structural Division 1967;93:381–99.

[13] Smith RJ, Adams PF. Experiments on Wide-Flange Beams under Moment Gradient. Structural Engineering Report No. 13, Dept. of Civil Engineering, University of Alberta, Edmonton, Canada, 1968.

[14] Lukey AF, Adams PF. Rotation Capacity of Beams under Moment Gradient. Journal of the Structural Division 1969;95:222–98.

[15] Tien YL, Wang ST. Local Buckling of Beams under Stress Gradient. Journal of the Structural Division 1979;105:1571–88.

[16] Mohebkhah A, Chegeni B. Flexural Capacity of Locally Buckled Steel I-Beams under Moment Gradient. The Open Construction & Building Technology Journal 2013;7:244–50.

[17] Han K-H, Lee C-H. Effects of moment gradient on elastic flange local buckling of I-shaped beams. International Journal of Steel Structures 2018;18:947–59. https://doi.org/10.1007/s13296-018-0039-5.

[18] Yang Z, Meng X, Walport F, Gardner L. Flexural capacity and local buckling half-wavelength of high strength steel tubular beams under moment gradients: An experimental study. Thin-Walled Structures 2024;195:111420. https://doi.org/10.1016/j.tws.2023.111420.

[19] Yang Z, Meng X, Walport F, Gardner L. Simulation and cross-section design of steel beams under moment gradients. Thin-Walled Structures 2025;209:112786. https://doi.org/10.1016/j.tws.2024.112786.

[20] Yang Z, Chen Y, Zhou F, Gardner L, Li G-Q. Testing and cross-section design of hot-rolled steel I-section beams under moment gradients. Engineering Structures 2025;338:120610. https://doi.org/10.1016/j.engstruct.2025.120610.

[21] Zhao O, Gardner L, Young B. Behaviour and design of stainless steel SHS and RHS beam-columns. Thin-Walled Structures 2016;106:330–45. https://doi.org/10.1016/j.tws.2016.04.018.

[22] Zhao O, Rossi B, Gardner L, Young B. Experimental and numerical studies of ferritic stainless steel tubular cross sections under combined compression and bending. Journal of Structural Engineering 2016;142:04015110. https://doi.org/10.1061/(ASCE)ST.1943-541X.0001366

[23] Wang F, Young B, Gardner L. Experimental study of square and rectangular CFDST sections with stainless steel outer tubes under axial compression. Journal of Structural Engineering 2019;145:04019139. https://doi.org/10.1061/(ASCE)ST.1943-541X.0002408.

[24] Chen Y, Zhou F, Zhang R, Cai Y. Experimental study on seismic behavior of welded H-section stainless steel beam-columns. Engineering Structures 2022;259:114105. https://doi.org/10.1016/j.engstruct.2022.114105.

[25] Chen Y, Zhou F, Zheng S, Li H-T, Su S. Cyclic behavior of cold-formed stainless steel sandwich tubular brace: An experimental investigation. Journal of Building Engineering 2024;96:110625. https://doi.org/10.1016/j.jobe.2024.110625.

[26] Gardner L, Yun X, Walport F. The continuous strength method – review and outlook. Engineering Structures 2023;275:114924. https://doi.org/10.1016/j.engstruct.2022.114924.

[27] European Committee for Standardization (CEN). EN 1993-1-4:2025, Eurocode 3 – Design of steel structures – Part 1-4: Stainless steel structures. Brussels: CEN; 2023.

[28] European Committee for Standardization (CEN). EN 1990:2023, Eurocode - Basis of Structural Design. Brussels: European Committee for Standardization (CEN); 2023.

[29] Li Z, Schafer B. Buckling Analysis of Cold-formed Steel Members with General Boundary Conditions Using CUFSM Conventional and Constrained Finite Strip Methods. CCFSS Proceedings of International Specialty Conference on Cold-Formed Steel Structures (1971 - 2018) 2010.

[30] European Committee for Standardization (CEN). EN ISO 13919-1:2019, Electron and laser-beam welded joints - Requirements and recommendations on quality levels for imperfections - Part 1: Steel, nickel, titanium and their alloys. Brussels: European Committee for Standardization (CEN); 2019.

[31] European Committee for Standardization (CEN). BS EN ISO 6892-1:2019, Metallic Materials: Tensile Testing — Method of Test at Room Temperature. Brussels: European Committee for Standardization (CEN); 2019.

[32] American Society for Testing and Materials (ASTM International). ASTM E8/E8M-24:2024, Standard Test Methods for Tension Testing of Metallic Materials. West Conshohocken, PA: ASTM International; 2024.

[33] Arrayago I, Real E, Gardner L. Description of stress–strain curves for stainless steel alloys. Materials & Design 2015;87:540–52. https://doi.org/10.1016/j.matdes.2015.08.001.

[34] European Committee for Standardization (CEN). prEN 1993-1-14:2023, Eurocode 3 – Design of steel structures – Part 1-14: Design assisted by finite element analysis. Brussels: CEN; 2023.

[35] Meng X, Gardner L. Testing of hot-finished high strength steel SHS and RHS under combined compression and bending. Thin-Walled Structures 2020;148:106262. https://doi.org/10.1016/j.tws.2019.106262.

[36] Meng X, Weber B, Nitawaki M, Gardner L. Optimisation and testing of wire arc additively manufactured steel stub columns. Thin-Walled Structures 2023;189:110857. https://doi.org/10.1016/j.tws.2023.110857.

[37] European Committee for Standardization (CEN). EN 1090-2:2018, Execution of Steel Structures and Aluminium Structures Part 2: Technical Requirements for Steel Structures, Brussels, 2018.

[38] Tebedge N, Alpsten G, Tall L. Residual-stress measurement by the sectioning method. Experimental Mechanics 1973;13:88–96. https://doi.org/10.1007/BF02322389.

[39] Kyvelou P, Huang C, Li J, Gardner L. Residual stresses in steel I-sections strengthened by wire arc additive manufacturing. Structures 2024;60:105828. https://doi.org/10.1016/j.istruc.2023.105828.

[40] Gardner L, Bu Y, Theofanous M. Laser-welded stainless steel I-sections: Residual stress measurements and column buckling tests. Engineering Structures 2016;127:536–48. https://doi.org/10.1016/j.engstruct.2016.08.057.

[41] Meng X, Gardner L. Cross-sectional behaviour of cold-formed high strength steel circular hollow sections. Thin-Walled Structures 2020;156:106822. https://doi.org/10.1016/j.tws.2020.106822.

[42] Saliba N, Gardner L. Experimental study of the shear response of lean duplex stainless steel plate girders. Engineering Structures 2013;46:375–91. https://doi.org/10.1016/j.engstruct.2012.07.029.

[43] Abaqus 2021 [software]. Dassault Systèmes 2021.

[44] Yun X, Gardner L, Boissonnade N. The continuous strength method for the design of hot-rolled steel cross-sections. Engineering Structures 2018;157:179–91. https://doi.org/10.1016/j.engstruct.2017.12.009.

[45] Theofanous M, Chan TM, Gardner L. Flexural behaviour of stainless steel oval hollow sections. Thin-Walled Structures 2009;47:776–87. https://doi.org/10.1016/j.tws.2009.01.001.

[46] Zhao O, Gardner L, Young B. Buckling of ferritic stainless steel members under combined axial compression and bending. Journal of Constructional Steel Research 2016;117:35–48. https://doi.org/10.1016/j.jcsr.2015.10.003.

[47] Kyvelou P, Gardner L, Nethercot DA. Finite element modelling of composite cold-formed steel flooring systems. Engineering Structures 2018;158:28–42. https://doi.org/10.1016/j.engstruct.2017.12.024.

[48] Lan X, Chen J, Chan T-M, Young B. The continuous strength method for the design of high strength steel tubular sections in compression. Engineering Structures 2018;162:177–87. https://doi.org/10.1016/j.engstruct.2018.02.010.

[49] Lan X, Chen J, Chan T-M, Young B. The continuous strength method for the design of high strength steel tubular sections in bending. Journal of Constructional Steel Research 2019;160:499–509. https://doi.org/10.1016/j.jcsr.2019.05.037.

[50] Kucukler M, Xing Z, Gardner L. Behaviour and design of stainless steel I-section columns in fire. Journal of Constructional Steel Research 2020;165:105890. https://doi.org/10.1016/j.jcsr.2019.105890.

[51] Ng KT, Gardner L. Buckling of stainless steel columns and beams in fire. Engineering Structures 2007;29:717–30. https://doi.org/10.1016/j.engstruct.2006.06.014.

[52] Afshan S, Zhao O, Gardner L. Standardised material properties for numerical parametric studies of stainless steel structures and buckling curves for tubular columns. Journal of Constructional Steel Research 2019;152:2–11. https://doi.org/10.1016/j.jcsr.2018.02.019.

[53] Yuan HX, Wang YQ, Shi YJ, Gardner L. Residual stress distributions in welded stainless steel sections. Thin-Walled Structures 2014;79:38–51. https://doi.org/10.1016/j.tws.2014.01.022.

[54] Fieber A, Gardner L, Macorini L. Formulae for determining elastic local buckling half-wavelengths of structural steel cross-sections. Journal of Constructional Steel Research 2019;159:493–506. https://doi.org/10.1016/j.jcsr.2019.04.037.

[55] Saliba N, Real E, Gardner L. Shear design recommendations for stainless steel plate girders. Engineering Structures 2014;59:220–8. https://doi.org/10.1016/j.engstruct.2013.10.016.

[56] Ashraf M, Gardner L, Nethercot DA. Structural stainless steel design: Resistance based on deformation capacity. Journal of Structural Engineering 2008;134:402–11. https://doi.org/10.1061/(ASCE)0733-9445(2008)134:3(402).

[57] Gardner, L. and Nethercot, D. A. (2004). Structural stainless steel design: A new approach. The Structural Engineer. 82(21), 21-28.

[58] Yuan HX, Wang YQ, Shi YJ, Gardner L. Stub column tests on stainless steel built-up sections. Thin-Walled Structures 2014;83:103–14. https://doi.org/10.1016/j.tws.2014.01.007.

[59] American Society of Civil Engineers (ASCE). ASCE/SEI 8-22: Specification for the Design of Cold-Formed Stainless Steel Structural Members. Reston, VA: ASCE; 2022.

[60] American Institute of Steel Construction (AISC). AISC 370: Specification for Structural Stainless Steel Buildings. Draft for public review. Chicago, IL: AISC; 2021.

[61] Walport, F., Kucukler, M. and Gardner, L. (2022). Stability design of stainless steel structures. Journal of Structural Engineering, ASCE. 148(1), 04021225.

[62] Fieber A, Gardner L, Macorini L. Structural steel design using second-order inelastic analysis with strain limits. Journal of Constructional Steel Research 2020;168:105980. https://doi.org/10.1016/j.jcsr.2020.105980.

[63] Kucukler M, Xing Z, Gardner L. Behaviour and design of stainless steel I-section columns in fire. Journal of Constructional Steel Research 2020;165:105890. https://doi.org/10.1016/j.jcsr.2019.105890.

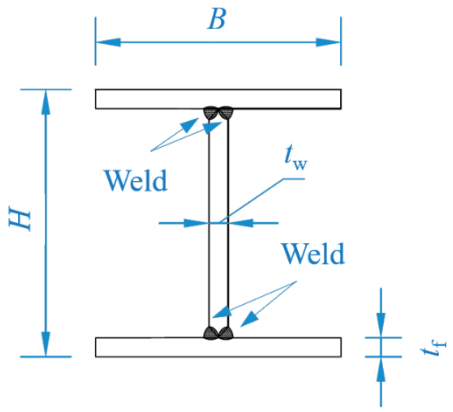
[64] Liew A, Gardner L. Ultimate capacity of structural steel cross-sections under compression, bending and combined loading. Structures 2015;1:2–11. https://doi.org/10.1016/j.istruc.2014.07.001.

[65] Quan C, Kucukler M, Gardner L. Out-of-plane stability design of steel beams by second-order inelastic analysis with strain limits. Thin-Walled Structures 2021;169:108352. https://doi.org/10.1016/j.tws.2021.108352.

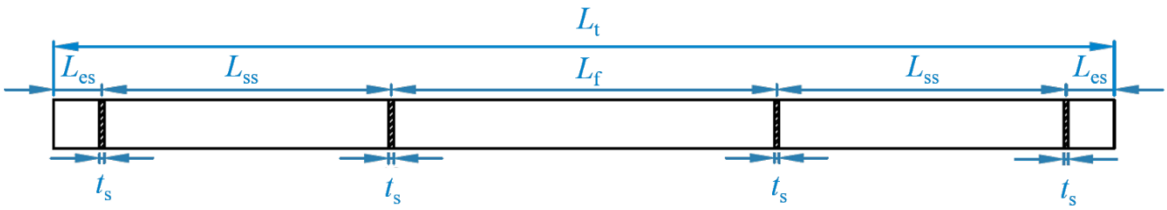
[66] Afshan S, Francis P, Baddoo NR, Gardner L. Reliability analysis of structural stainless steel design provisions. Journal of Constructional Steel Research 2015;114:293–304. https://doi.org/10.1016/j.jcsr.2015.08.012.

[67] Walport F, Chan HU, Nethercot DA, Gardner L. Design of stainless steel structural systems by GMNIA with strain limits. Engineering Structures 2023;276:115339. https://doi.org/10.1016/j.engstruct.2022.115339.

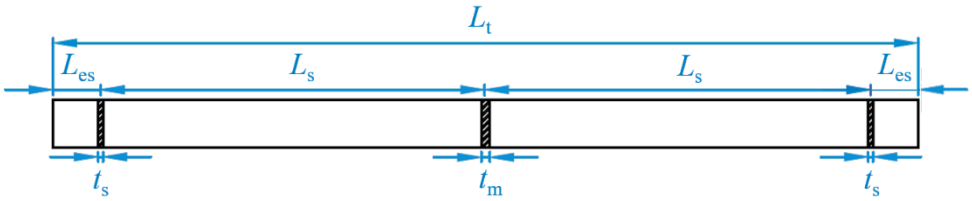
[68] Meza FJ, Baddoo N, Gardner L. Derivation of stainless steel material factors for european and U.S. design standards. Journal of Constructional Steel Research 2024;213:108383. https://doi.org/10.1016/j.jcsr.2023.108383.



(a) I-section dimensions

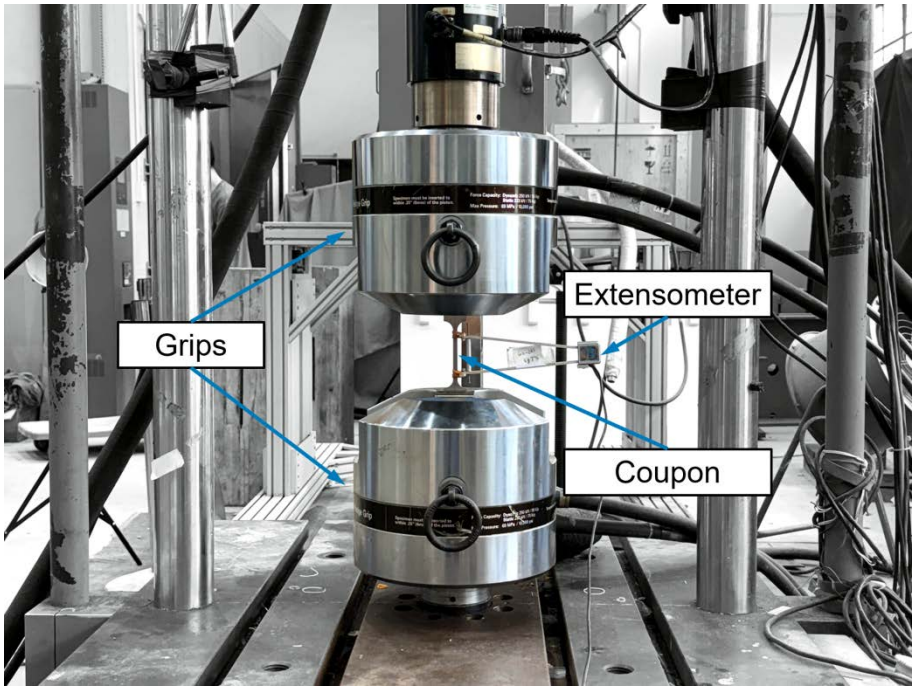


(b) Longitudinal dimensions of S4 series

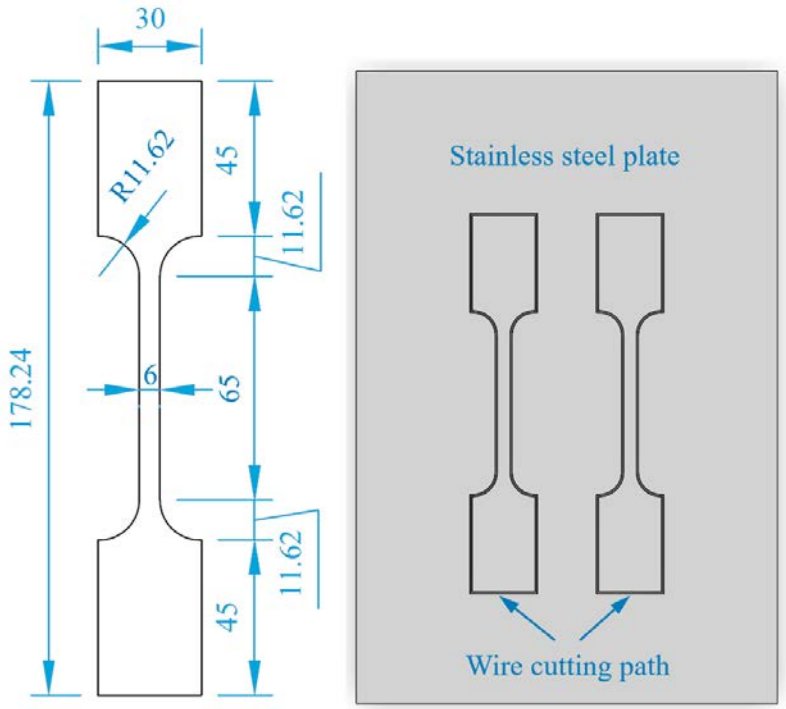


(c) Longitudinal dimensions of S3 series

Figure 1 Notation for geometric parameters of beam specimens.

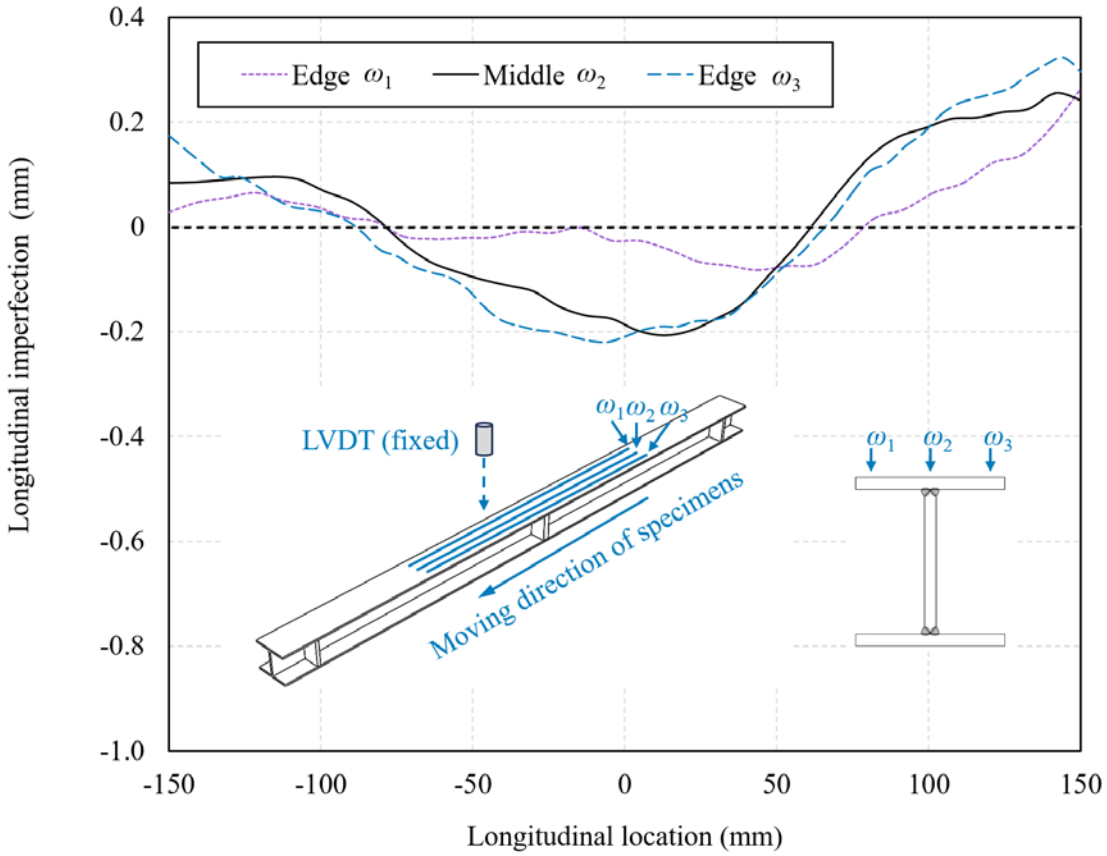


(a) Test setup



(b) Dimensions in mm and extraction regions of coupons

Figure 2 Tensile coupon test setup and details of coupons.

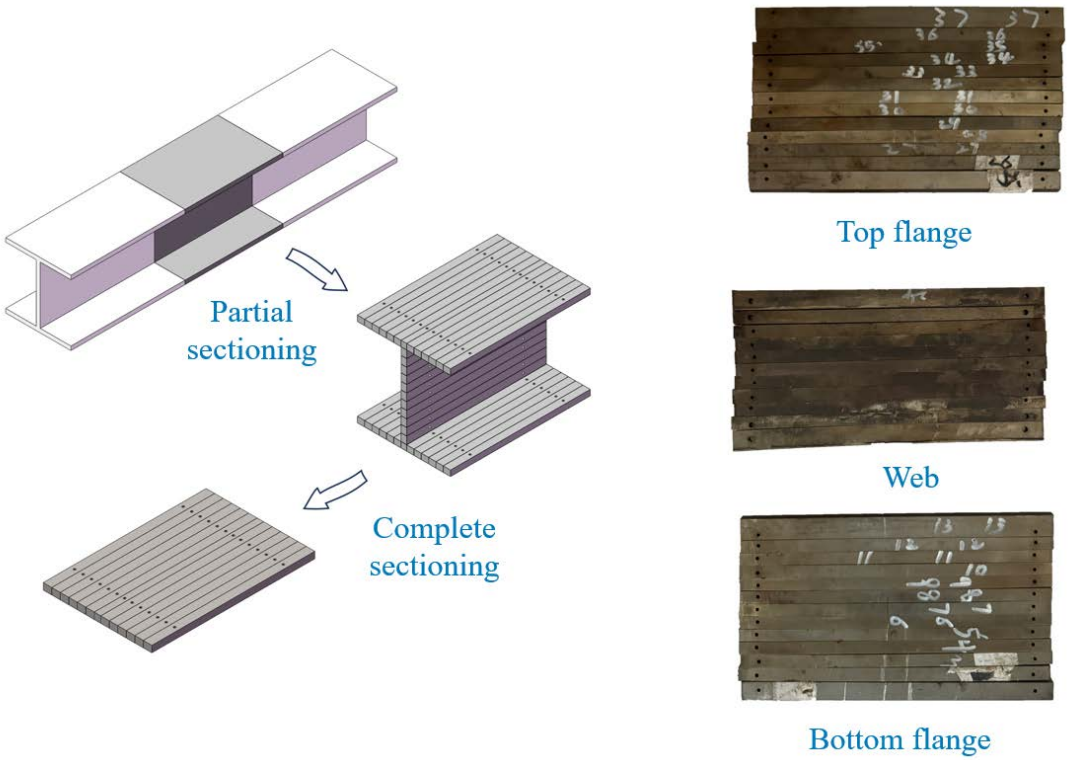


742

743 Figure 3 Typical distribution of measured longitudinal imperfections in the top flange of

744 specimen S3-2.

745

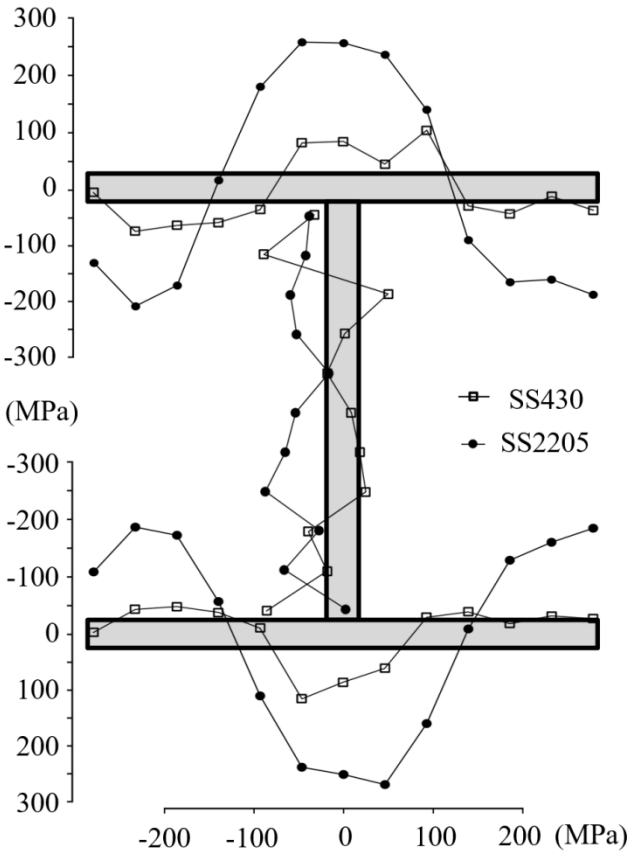


746

747 Figure 4 Schematic view of the sectioning method and longitudinal strips after cutting.

748

749

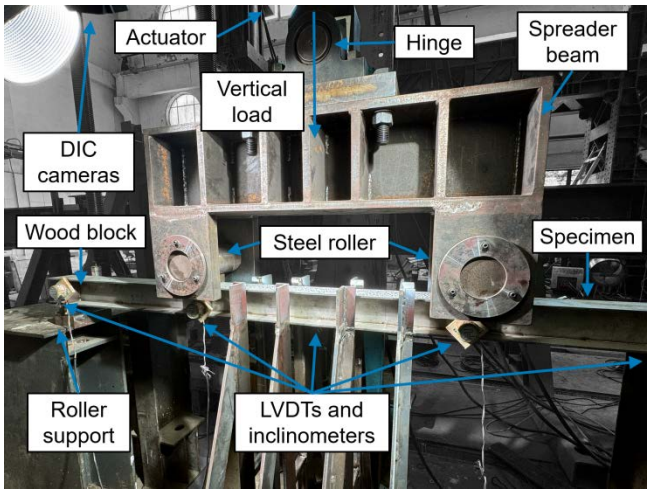


750

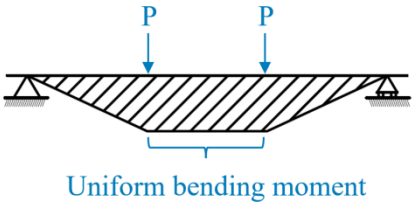
751 Figure 5 Measured residual stress distributions (positive = tension, negative = compression).

752

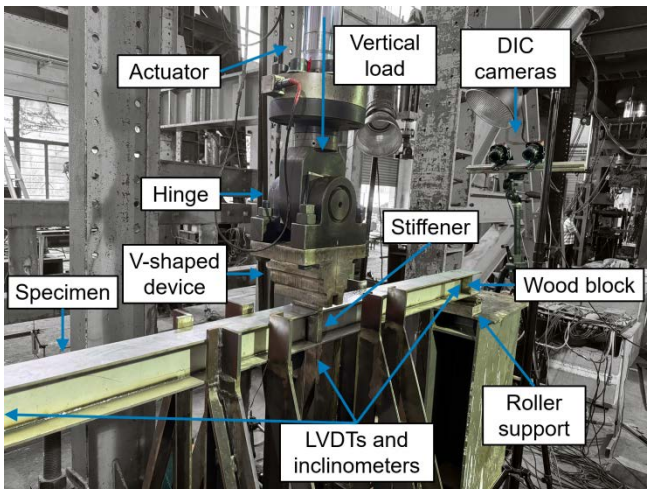
753



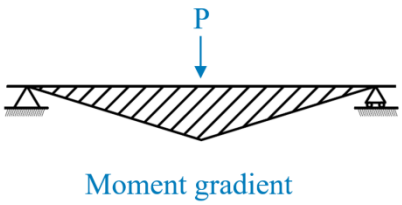
(a) Test setup for four-point bending tests



(b) Bending moment diagram for four-point bending tests

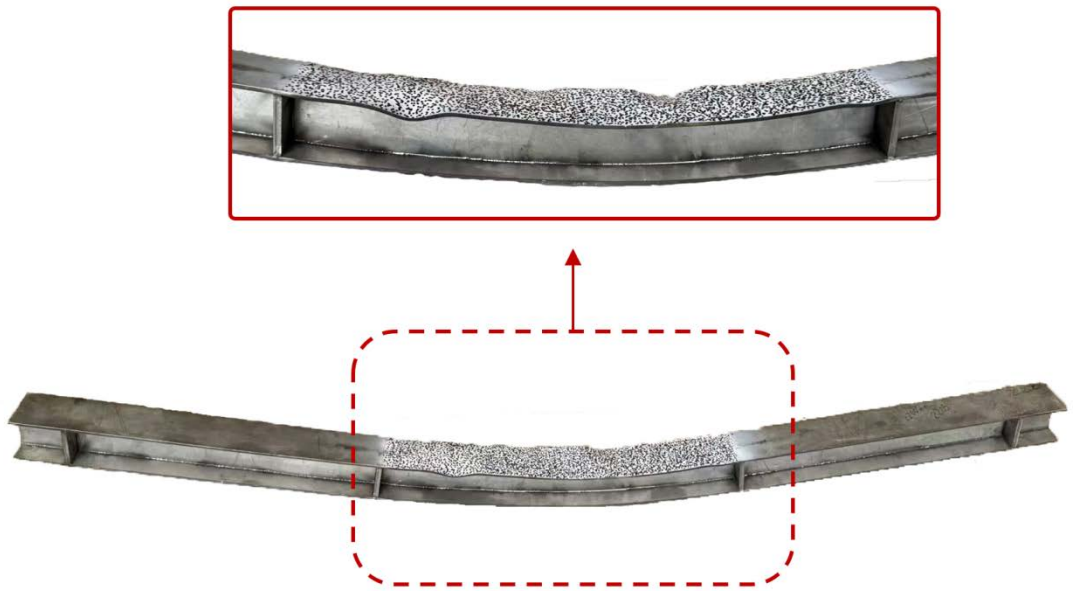


(c) Test setup for three-point bending tests

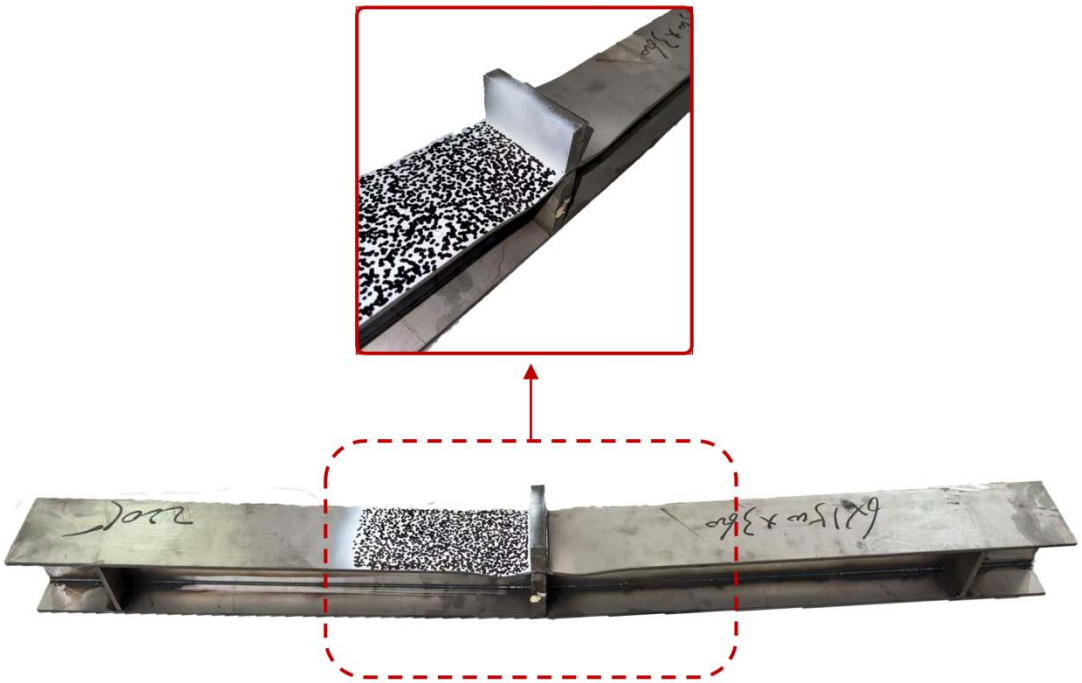


(d) Bending moment diagram for three-point bending tests

Figure 6 Test setup, measurement system and bending moment diagrams for four- and stiffened three-point bending tests.

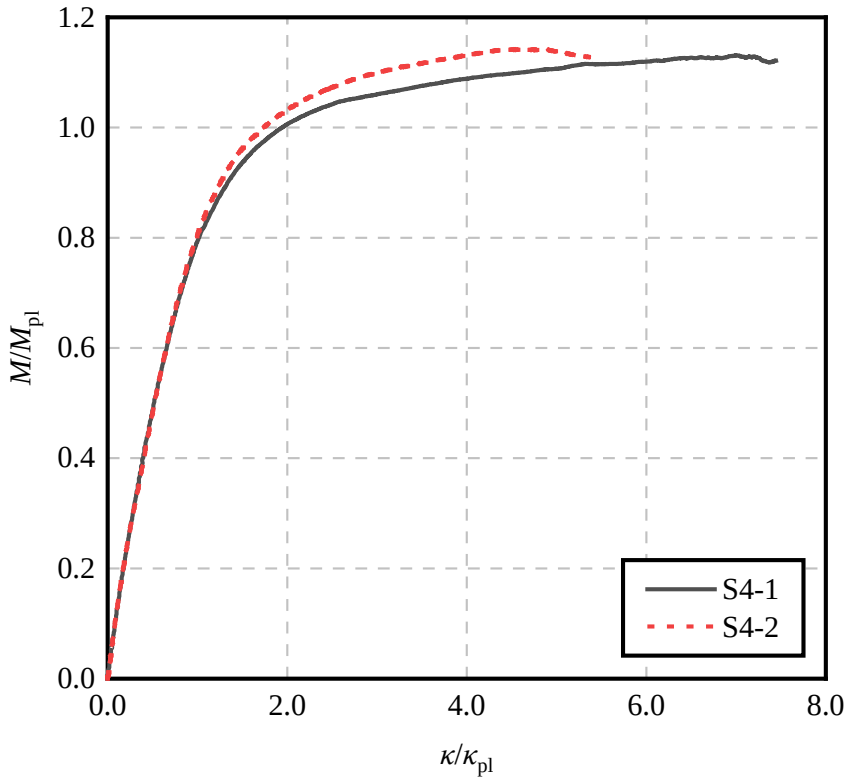


(a) S4-1

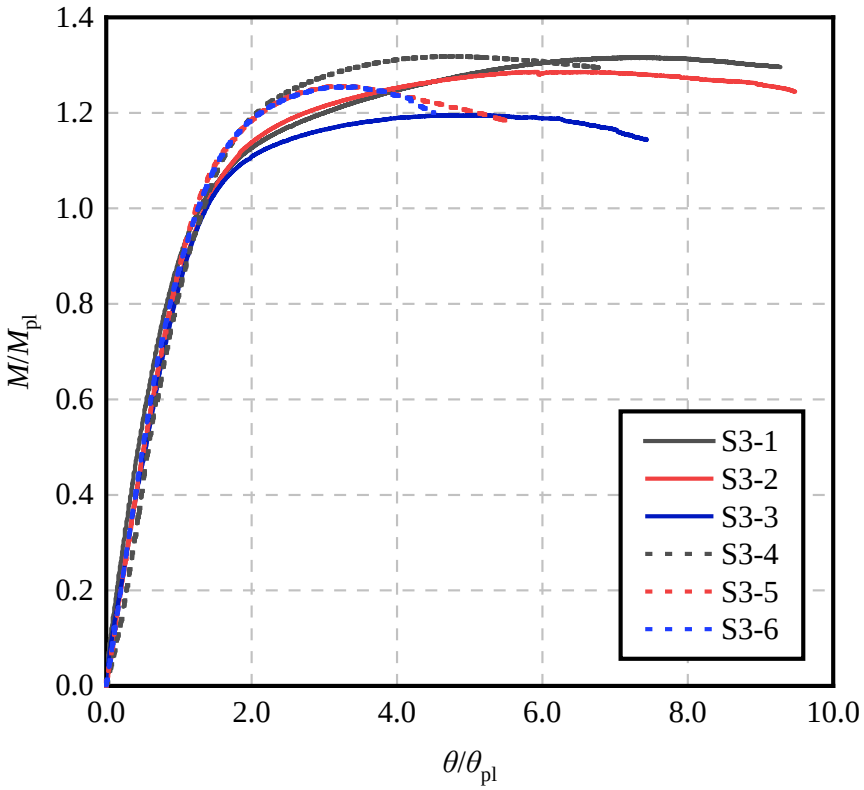


(b) S3-4

Figure 7 Typical failure modes of specimens under four- and stiffened three-point bending.

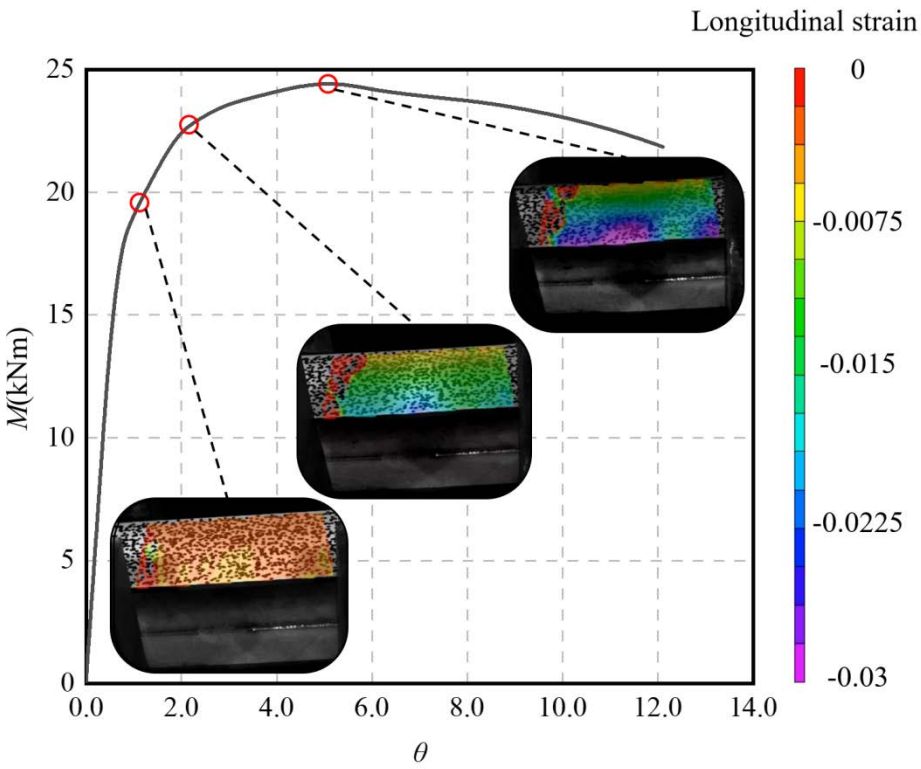


(a) S4 series

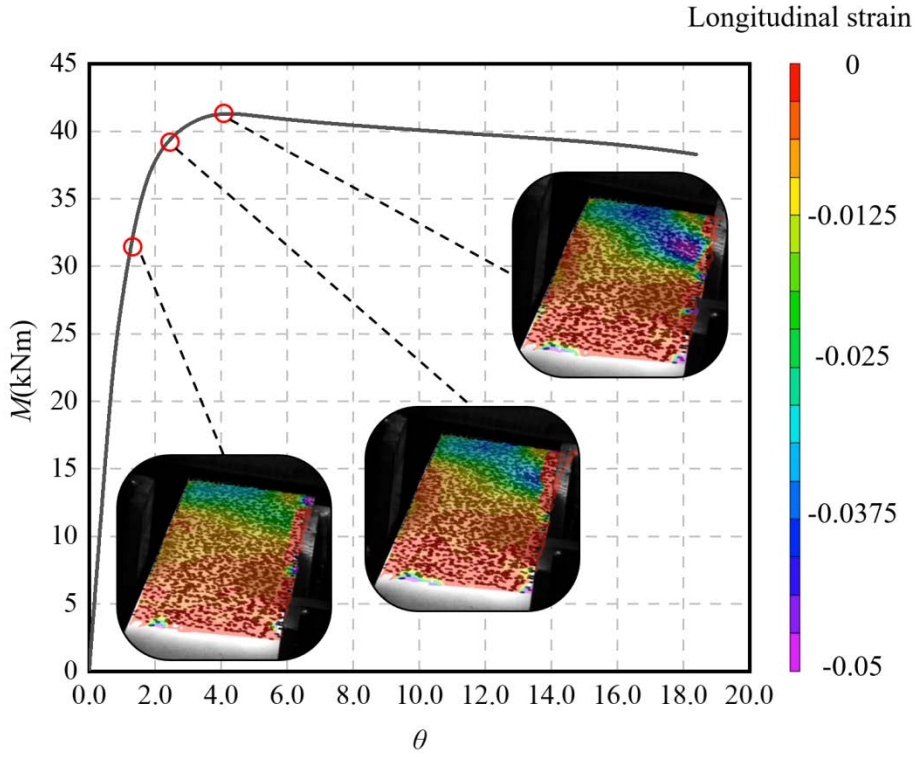


(b) S3 series

Figure 8 Normalised mid-span moment against average curvature and average end rotation curves for four- and stiffened three-point bending tests.

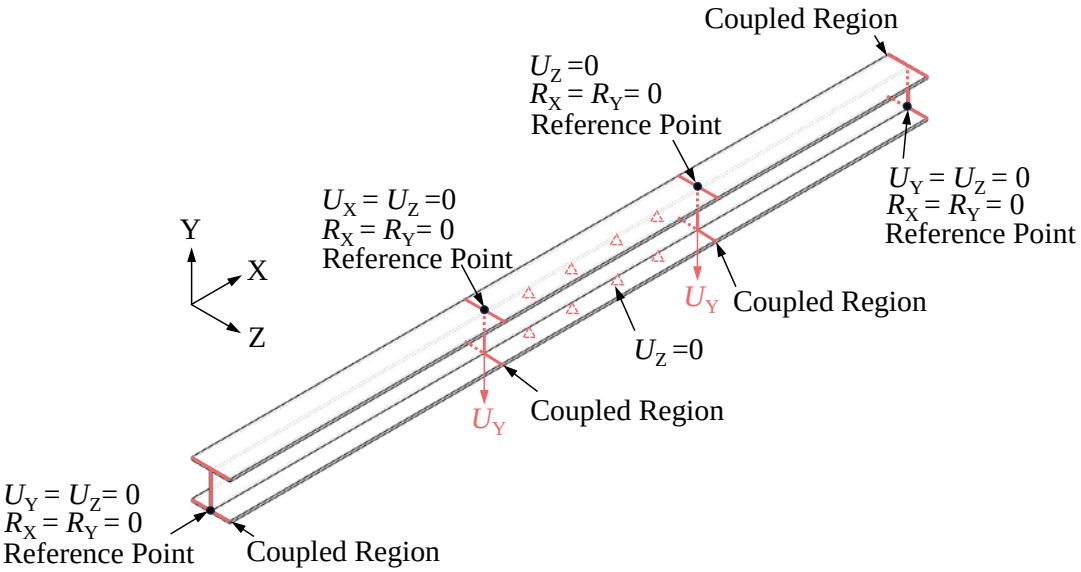


(a) S4-1

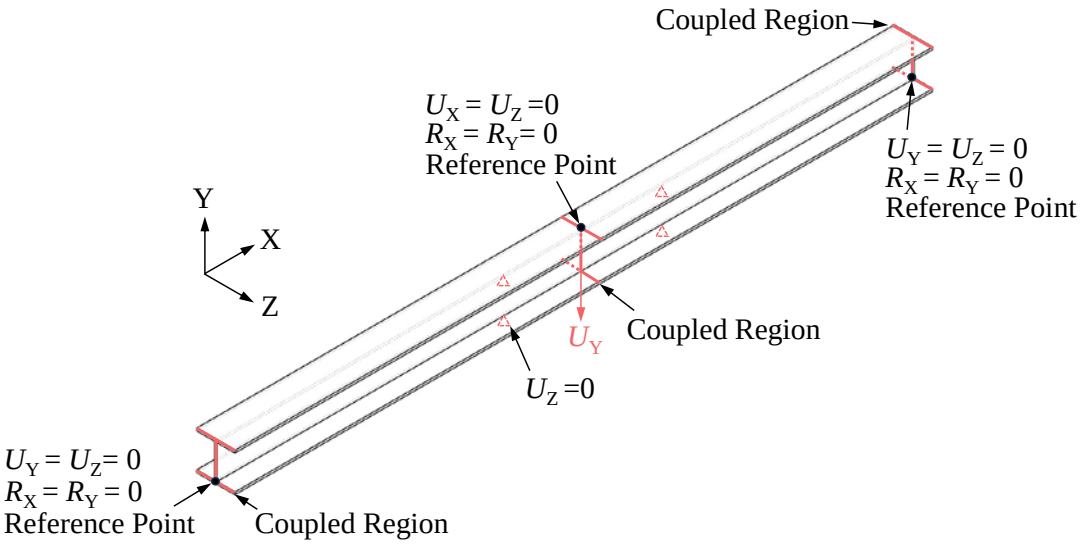


(b) S3-4

Figure 9 Typical development of longitudinal strain in compression flange of specimens monitored under four- and stiffened three-point bending, as determined from DIC.

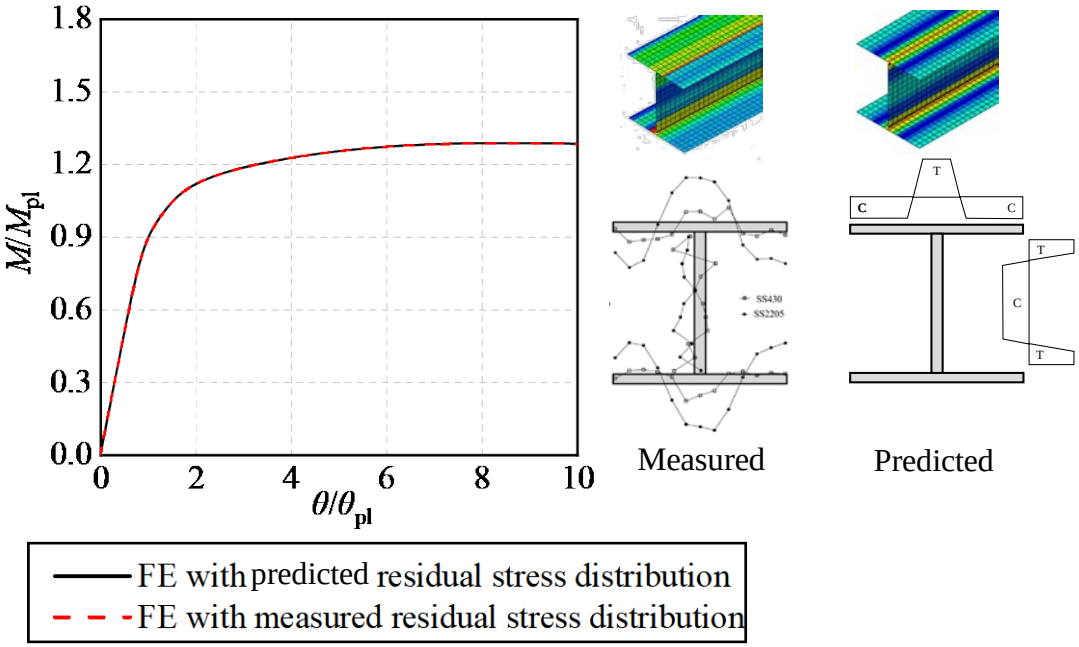


(a) I-section beam under four-point bending



(b) Stiffened I-section beam under three-point bending

Figure 10 Boundary conditions employed in FE models for validation.



783

784 Figure 11 Comparison of typical load–deformation curves for measured residual stresses and

785 predicted residual stress distributions.

786

787

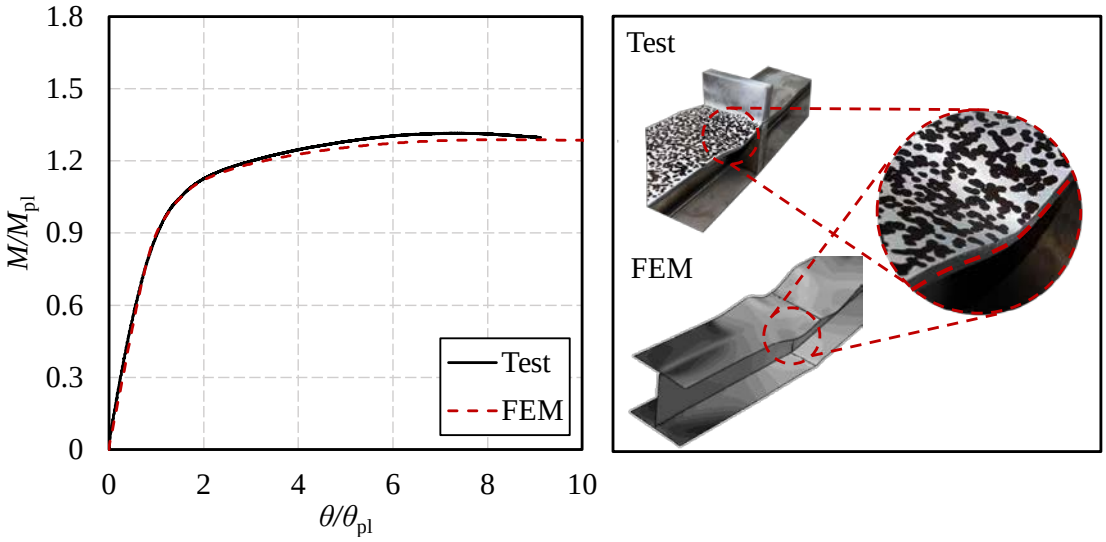
788

789

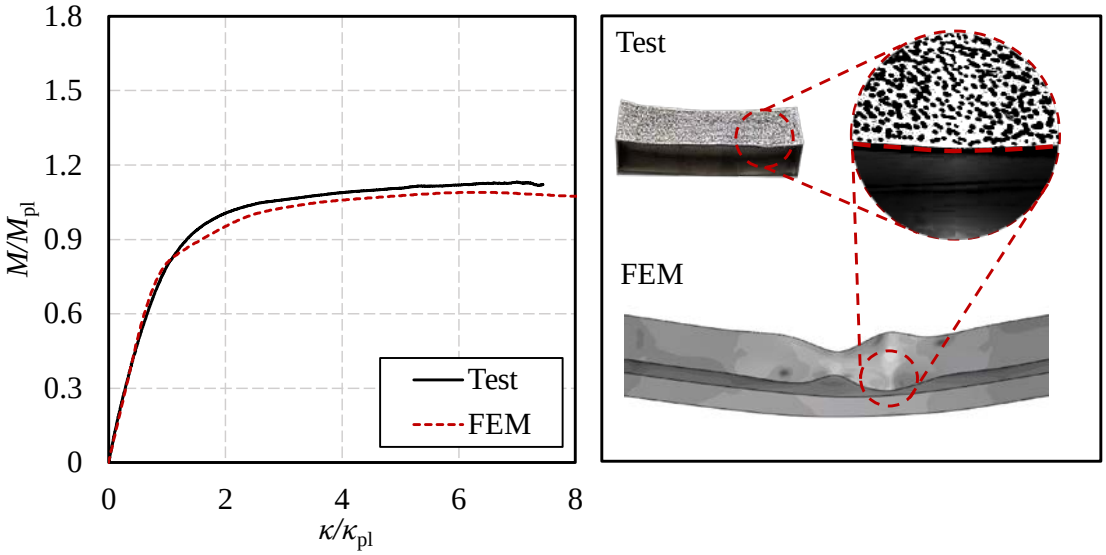
790

791

792

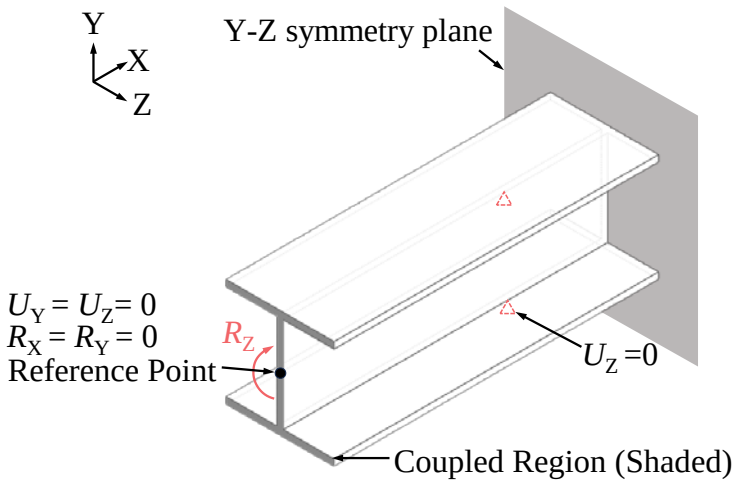


(a) S3-1

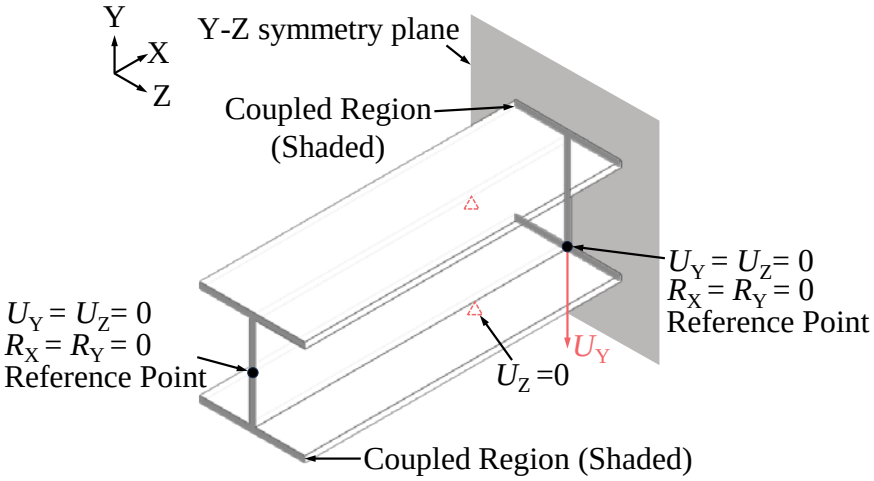


(b) S4-1

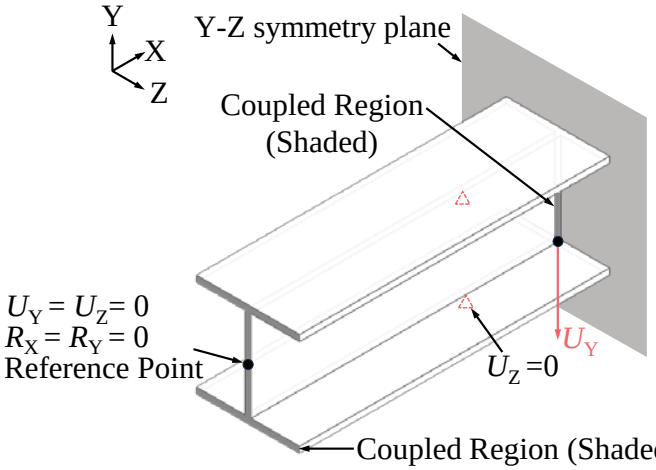
Figure 12 Comparison of typical load-deformation curves and failure modes for I-sections from tests and FE analysis.



(a) I-section under uniform bending



(b) Stiffened I-section under three-point bending



(c) Unstiffened I-section under three-point bending

Figure 13 Boundary conditions of FE models employed for parametric studies.

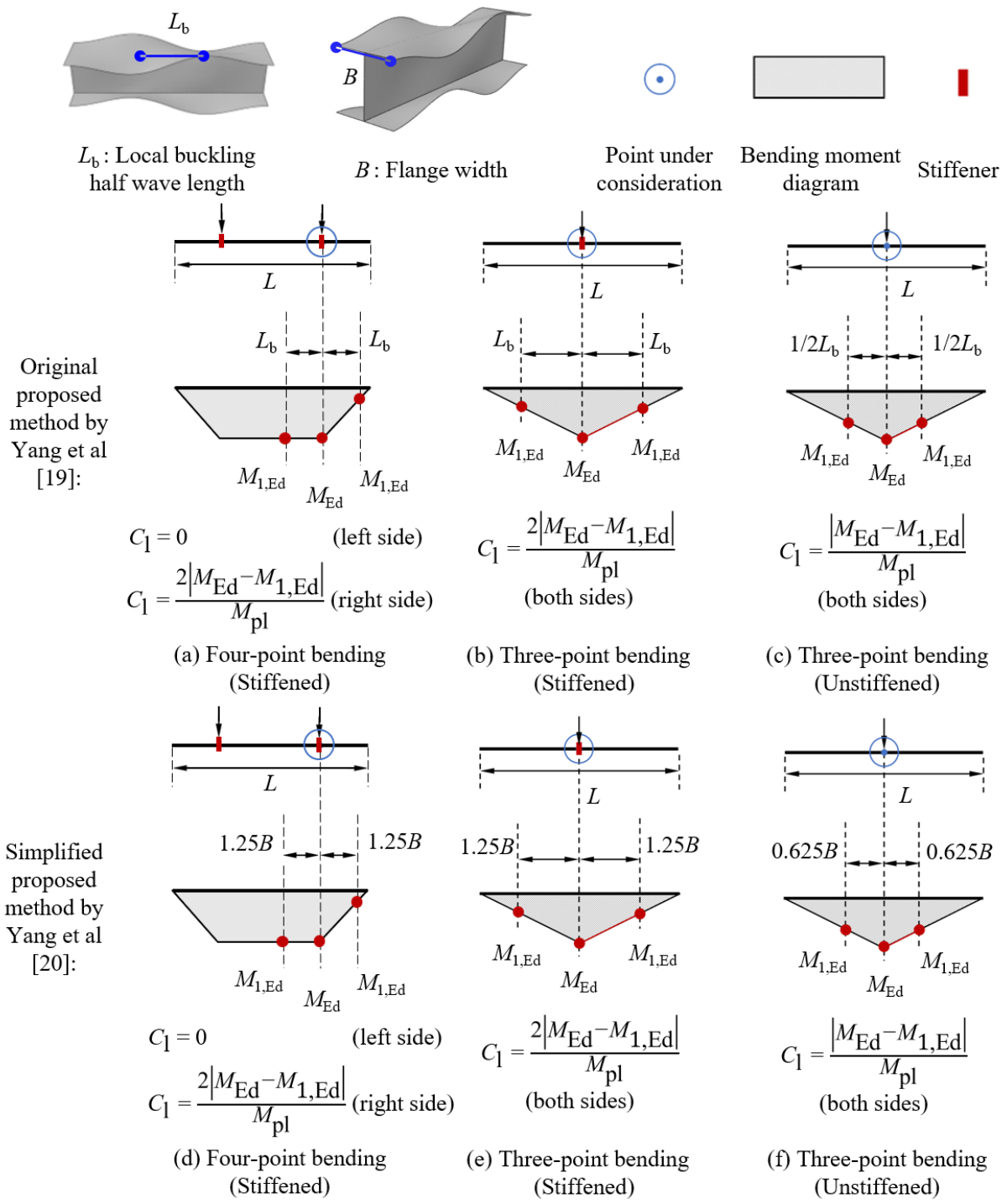


Figure 14 Determination of C_1 at point under consideration using local buckling half-wavelength L_b and a proportion of the flange width B to define second point(s) at which bending moments are determined.

EN 1993-1-4:2025

1. Web shearing buckling & design shear resistance check

$$h_w/t_w \leqslant 52\,\varepsilon/\eta \;\;\&\;\; V_{Ed}<V_{pl,Rd}$$

2. Calculate design full cross-section moment resistance $M_{c,Rd}$

$$M_{c,Rd}=\frac{M_{c,Rk}}{\gamma_{M0}}$$

$$M_{c,Rk}=Wf_y$$

$$W=\begin{cases}W_{pl} & \text{for Class 1 and 2}\\ W_{el} & \text{for Class 3}\\ W_{eff} & \text{for Class 4}\end{cases}$$

3. Calculate design plastic moment resistance $M_{V,Rd}$ by considering shear force

$$M_{V,Rd}=\frac{M_{V,Rk}}{\gamma_{M0}}$$

$$M_{V,Rk}=\begin{cases}W_{pl}f_y & \text{For } V_{Ed}\leqslant\eta_V V_{pl,Rd}\\ W_{pl,V}f_{y,red}+W_{pl,nV}f_y & \text{For } \eta_V V_{pl,Rd}<V_{Ed}\leqslant V_{pl,Rd}\end{cases}$$

4. Check if $M_{Ed}\leqslant \min(M_{c,Rd}, M_{V,Rd})$

Proposed method by Yang et al.

1. Web shearing buckling & design shear resistance check

$$h_w/t_w \leqslant 52\,\varepsilon/\eta \;\;\&\;\; V_{Ed}<V_{pl,Rd}$$

2. Calculate the modified resistance $M_{mod,V,Rd}$ by considering moment gradient effects

$$M_{mod,V,Rd}=\frac{M_{mod,V,Rk}}{\gamma_{M0}}$$

$$W=\begin{cases}W_{pl} & \text{for Class 1 and 2}\\ W_{el} & \text{for Class 3}\\ W_{eff} & \text{for Class 4}\end{cases}$$

Original proposed method by Yang et al [19]: C_1 was calculated with L_b

Simplified proposed method by Yang et al [20]: C_1 was calculated with B

$$\kappa_{C1}=0.15C_1+1$$

$$M_{mod,V,Rk}=\begin{cases}\kappa_{C1}Wf_y & \text{For } V_{Ed}\leqslant\eta_V V_{pl,Rd}\\ \kappa_{C1}\left(W_V f_{y,red}+W_{nV}f_y\right) & \text{For } \eta_V V_{pl,Rd}<V_{Ed}\leqslant V_{pl,Rd}\end{cases}$$

3. Check if $M_{Ed}\leqslant M_{mod,V,Rd}$

Figure 15 Workflows of different design approaches for stainless steel beams under combined bending and shear.

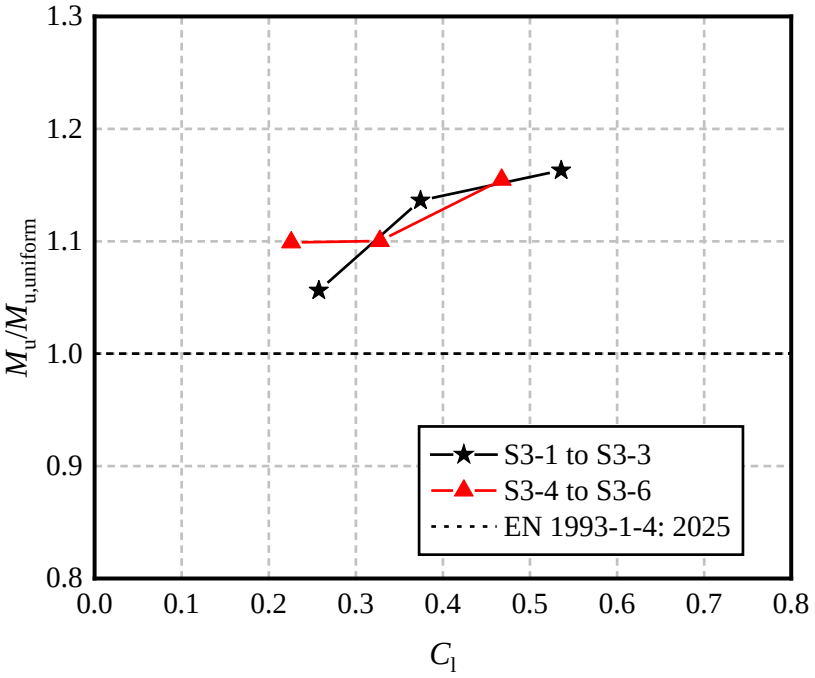


Figure 16 Test results showing values of M_u / $M_{u,uniform}$ versus local moment gradient parameter C_l for specimens under stiffened three-point bending.

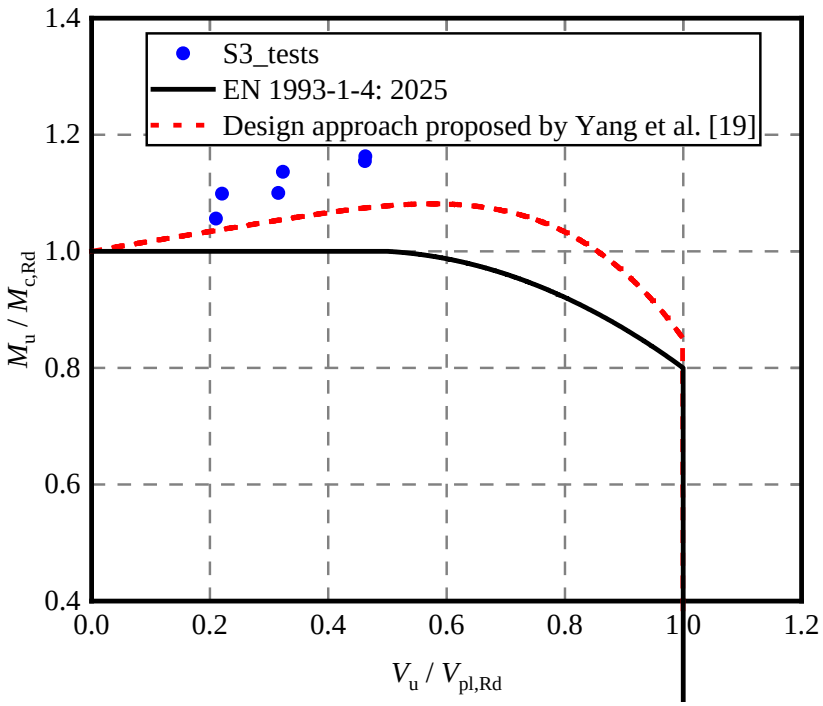
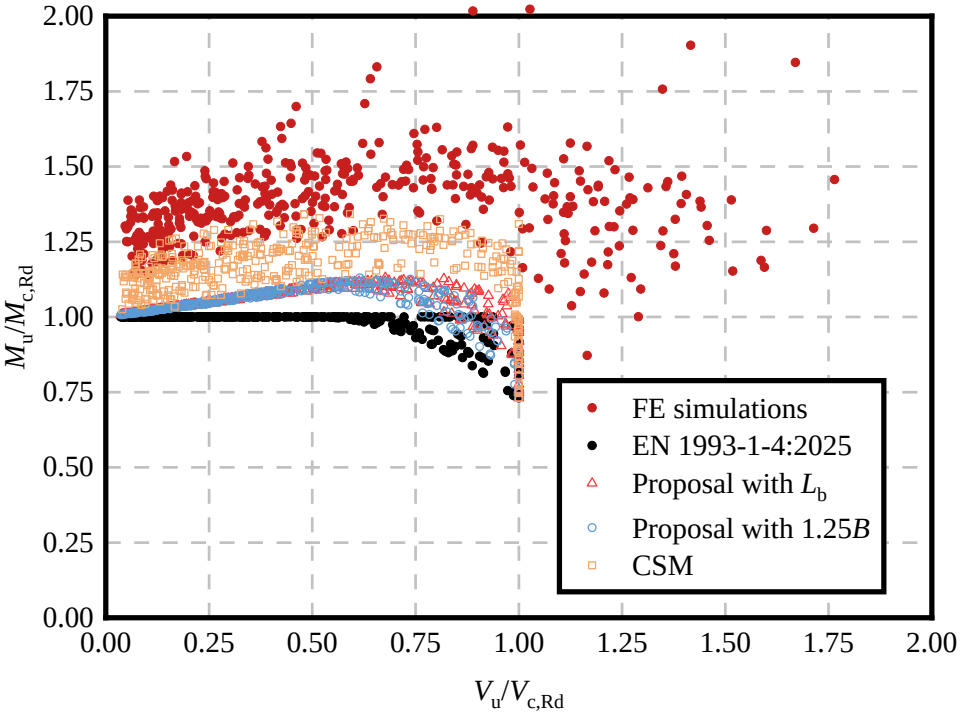
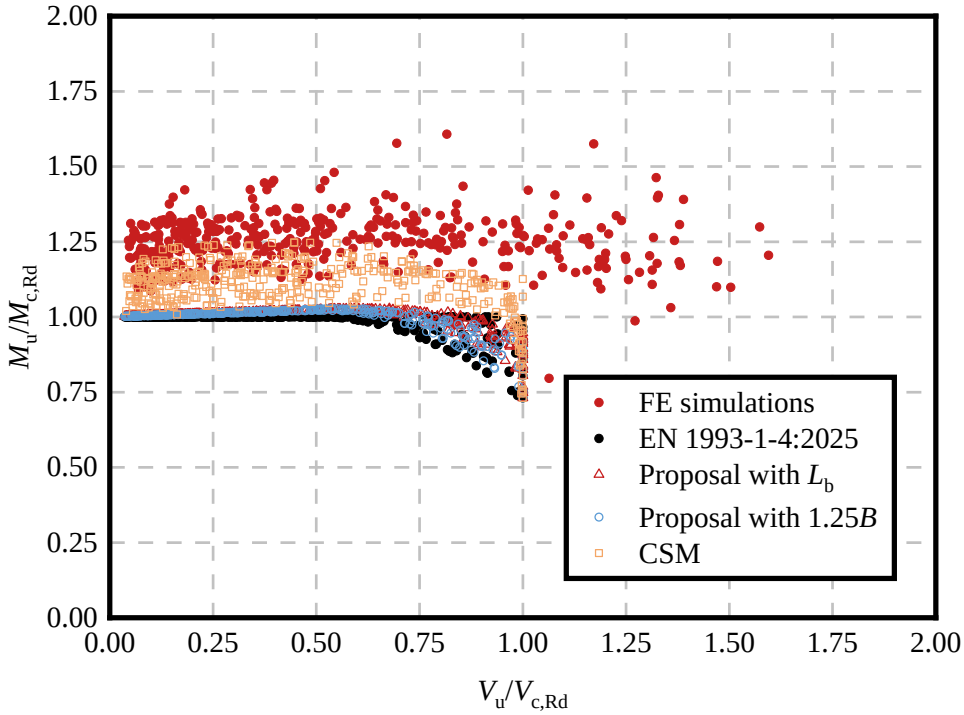


Figure 17 Comparison of test results with EC3 and proposed moment-shear interaction curves.



(a) Stiffened three-point bending



(b) Unstiffened three-point bending

Figure 18 Comparisons of FE normalised ultimate moment against shear force with design provisions in EC3, proposed design approach using L_b, simplified design approach using 1.25B and proposed CSM design approach with moment gradients.

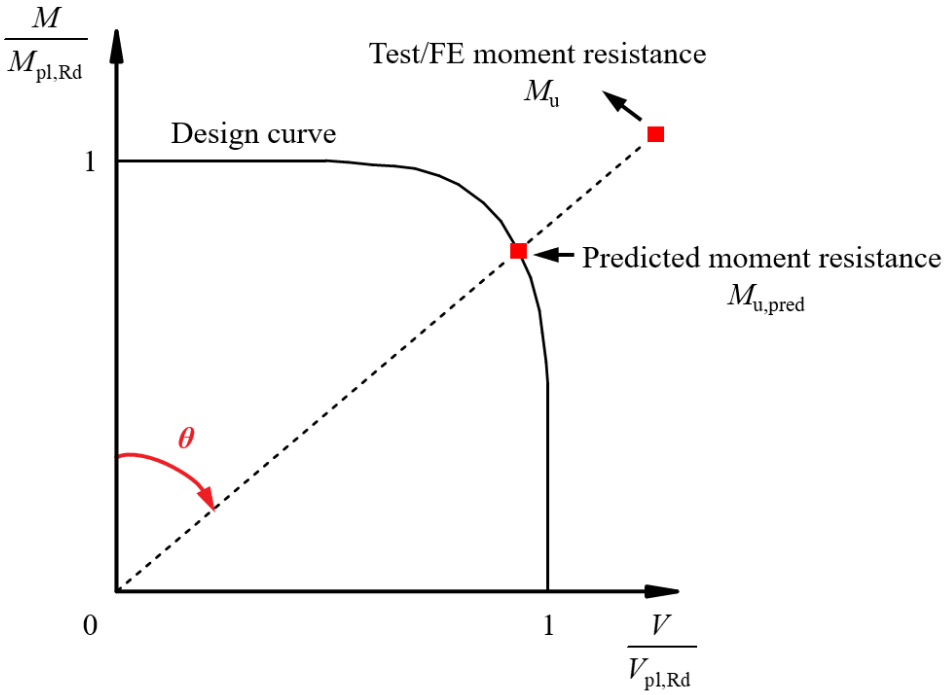
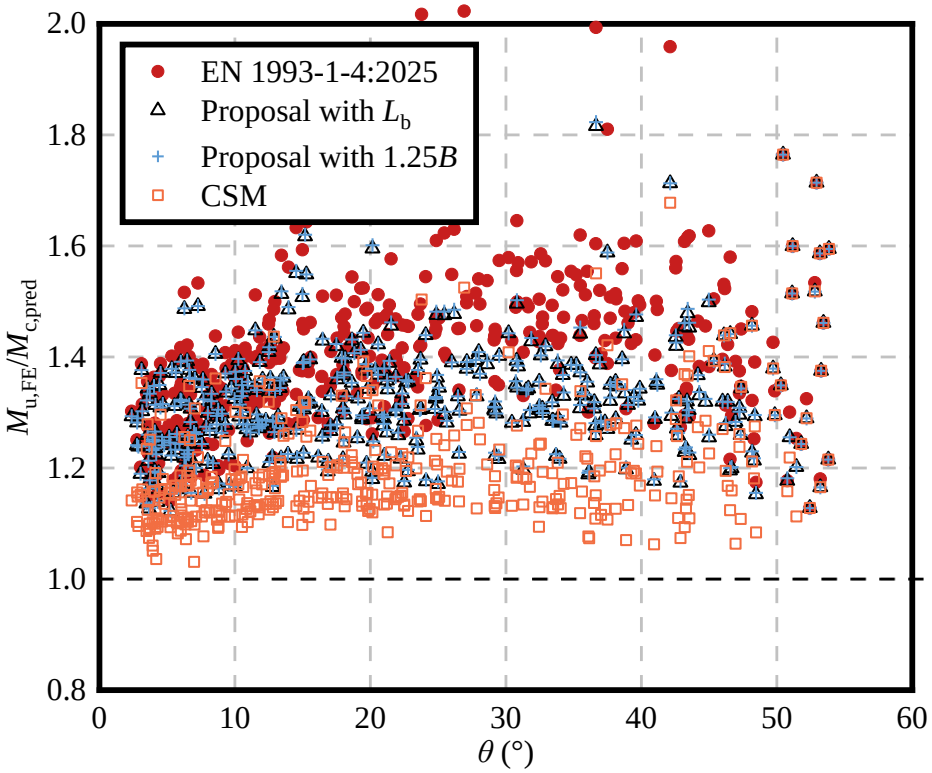
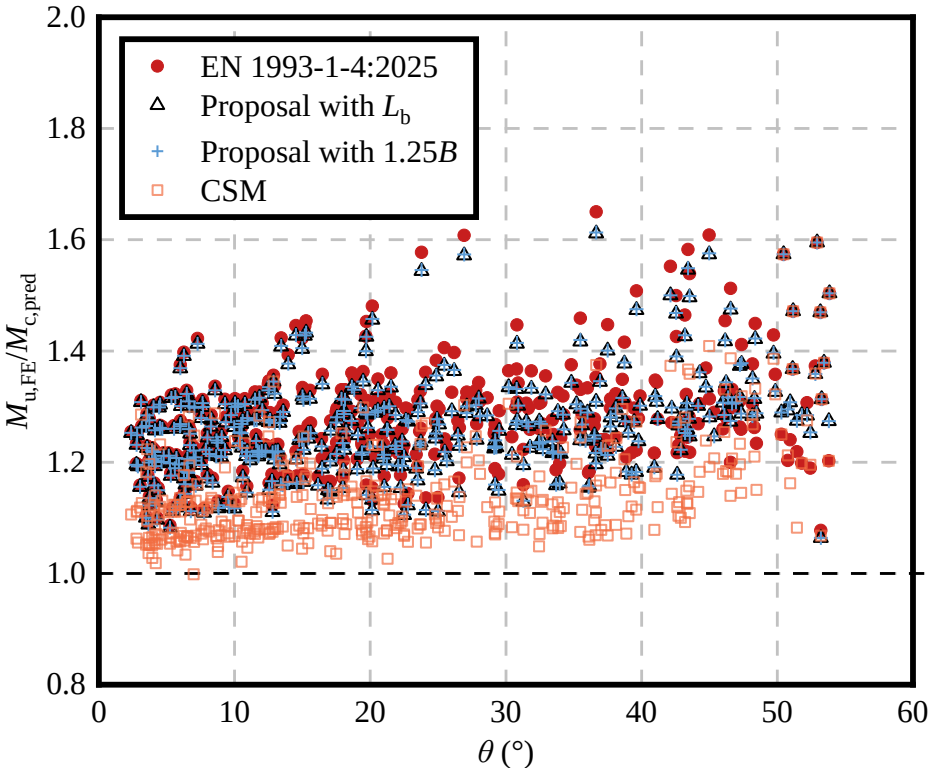


Figure 19 Definition of normalised shear-moment ratio θ.



(a) Stiffened three-point bending



(b) Unstiffened three-point bending

Figure 20 Ratios of FE to predicted resistances against shear-moment angle for design provisions in EC3, proposed design approach using L_b, simplified design approach using 1.25B and proposed CSM design approach with moment gradients.

30 Table 1 Measured geometric properties of stainless steel I-section beams.

Specimen ID	Grade	H (mm)	B (mm)	t_f (mm)	t_w (mm)	L_s or L_f (mm)	L_t (mm)	$\bar{\lambda}_{p,cs}$
S4-1	SS430	99.20	99.47	5.82	5.86	800	2197	0.39
S4-2	SS2205	98.88	99.40	5.85	5.99	800	2197	0.47
S3-1	SS430	98.69	99.66	5.81	5.85	500	1220	0.39
S3-2	SS430	98.76	99.73	5.80	5.90	700	1618	0.39
S3-3	SS430	99.14	99.64	5.90	5.91	1000	2216	0.39
S3-4	SS2205	99.31	99.14	5.86	5.95	500	1216	0.47
S3-5	SS2205	98.90	99.51	5.85	5.84	700	1617	0.47
S3-6	SS2205	98.89	99.40	5.85	5.99	1000	2216	0.47

31

32

33 Table 2 Measured material properties of SS430 and SS2205 stainless steel plate.

Grade	E (MPa)	f_y (MPa)	f_u (MPa)	ε_u (%)	ε_f (%)	n	m
SS430	-	353.9	456.8	9.48	12.33	2.55	3.71
	221100	340.7	447.9	11.41	19.33	2.90	3.66
SS2205	225100	501.2	728.0	23.52	35.40	2.28	3.41
	219500	508.1	737.4	26.13	37.88	1.32	3.41

34

35

Table 3 Longitudinal imperfection magnitudes of stainless steel I-section beams (unit: mm).

Specimen ID	ω_{1m}	ω_{2m}	ω_{3m}
S4-1	0.35	0.30	0.19
S4-2	0.21	0.22	0.08
S3-1	0.33	0.25	0.41
S3-2	0.27	0.35	0.48
S3-3	0.14	0.18	0.08
S3-4	0.16	0.34	0.32
S3-5	0.44	0.44	0.31
S3-6	0.49	0.17	0.33

Table 4 Summary of key results of tests.

Bending Configuration	Specimen ID	M_{pl} (kNm)	θ_{pl} (°) or κ_{pl} ($\times 10^{-4}$mm^{-1})	M_u (kNm)	θ_u (°) or κ_u ($\times 10^{-4}$mm^{-1})	M_u/M_{pl}	θ_u/θ_{pl} or κ_u/κ_{pl}
Four-point bending	S4-1	22.40	0.352	25.36	2.465	1.132	7.003
	S4-2	33.61	0.520	38.38	2.511	1.142	4.829
Stiffened three-point bending	S3-1	22.08	0.506	29.06	3.589	1.316	7.093
	S3-2	22.05	0.708	28.36	4.177	1.286	5.900
	S3-3	22.38	1.012	26.74	4.656	1.195	4.601
	S3-4	32.77	0.747	43.19	3.416	1.318	4.573
	S3-5	32.88	1.045	41.30	3.343	1.256	3.199
	S3-6	32.68	1.496	41.01	4.792	1.255	3.203

Table 5. Mesh sensitivity analysis results.

Mesh size	b_f /4	b_f /8	b_f /12	b_f /16	b_f /32
$M_{u,FEM}/M_{pl}$	1.363	1.327	1.320	1.316	1.314

69 Table 6 Comparison of results from benchmark FE models and tests.

Loading configuration	Specimen ID	$M_{\mathrm{u,test}}/M_{\mathrm{u,FEM}}$
Four-point bending	S4-1	1.038
	S4-2	1.033
	Mean	1.036
	COV	0.002
Stiffened three-point bending	S3-1	1.022
	S3-2	1.030
	S3-3	0.984
	S3-4	1.020
	S3-5	1.001
	S3-6	1.033
	Mean	1.015
	COV	0.017

70

71

72 Table 7 Material properties utilised in parametric studies.

Material type	f_y (MPa)	f_u (MPa)	ε_u	n	m
Austenitic	280	580	0.5	9.1	2.3
Ferritic	320	480	0.16	17.2	2.8
Duplex	530	770	0.3	9.3	3.6

73

74

75 Table 8 Comparison of results from FE models and design predictions.

Loading configuration	Numbers of data points	Evaluation parameter	$M_u/M_{u,pred}$			
			EN 1993 1-4: 2025	Proposal with L_b	Proposal with 1.25B	CSM
Stiffened three-point bending	409	Mean	1.401	1.321	1.323	1.197
		CoV	0.095	0.082	0.082	0.088
Unstiffened three-point bending	409	Mean	1.274	1.260	1.261	1.140
		CoV	0.072	0.070	0.070	0.076

76

77

78 Table 9 Key statistical parameters of material properties according to Afshan et al. [66].

Steel grade	$f_{y,mean}/f_{y,nom}$	$f_{u,mean}/f_{u,nom}$	V_{fy}
Austenitic	1.3	1.1	0.060
Ferritic	1.2	1.1	0.045
Duplex	1.1	1.1	0.030

79

80

Table 10 Key statistical parameters of geometric properties according to Afshan et al. [65].

Geometric parameter X	X_{mean}/X_{nom}	V_X
H	1.0141	0.0364
B	0.9977	0.0132
t_f	0.9994	0.0182
t_w	0.9991	0.0151

Table 11 Reliability analysis of beams under combined moment and shear.

Loading configurations	Design approach	No. of data points for each group	b	V_δ	V_r [1]	γ^*_{M0}	$\gamma^*_{M0}/\gamma_{M0}$
Stiffened I-section	Original EN 1993-1-4:2025	409	1.401	0.092	0.106	0.834	0.758
	Modified EN 1993-1-4:2025	409	1.323	0.078	0.094	0.851	0.774
	Modified CSM expressions	409	1.197	0.082	0.095	0.945	0.859
Unstiffened I-section	Original EN 1993-1-4:2025	409	1.274	0.070	0.088	0.865	0.787
	Modified EN 1993-1-4:2025	409	1.261	0.069	0.086	0.872	0.792
	Modified CSM expressions	409	1.140	0.072	0.087	0.967	0.879

[1] Parameters vary for each data point and the mean values are displayed.